KONA Powder and Particle Journal No. 40 (2023) 124–148/https://doi.org/10.14356/kona.2023004 Review Paper

Functionalized Graphitic Carbon Nitrides for Photocatalytic H_2O_2 Production: Desired Properties Leading to Rational Catalyst Design †

Zhengyuan Teng, Wenan Cai and Teruhisa Ohno *

Department of Applied Chemistry, Faculty of Engineering, Kyushu Institute of Technology, Japan

Abstract

Photocatalytic H_2O_2 production based on graphitic carbon nitride (g-C_3N_4) materials has been attracting increasing attention. However, it is difficult to reveal the inner relationships among the structure, properties and performance of a g-C_3N_4-based photocatalyst by simply summarizing preparation methods, properties and performances in previous works. In this review, the three most important issues for improving H_2O_2 generation based on the band diagram and physicochemical properties of pristine g-C_3N_4 are proposed. Improvement of the charge separation, promotion of the light absorption and introduction of active sites for 2e⁻ oxygen reduction reaction to suppress side reactions are the most three attractive strategies for enhancing the activities. Following discussion of these strategies, representative functionalization methods are summarized on the basis of the most desired properties for improving the photocatalytic activities for H_2O_2 production. Other influence factors for improving H_2O_2 production such as addition of electron donors and adjustment of pH value of the solution are also discussed. Future challenges for photocatalytic H_2O_2 based on g-C_3N_4 materials are also summarized to provide future directions in this field.

Keywords: carbon nitride, photocatalysis, functionalization, H_2O_2

1. Introduction

H_2O_2 has been recognized as one of the 100 most important chemicals worldwide (Jones C.W., 1999; Pesterfield L., 2009). The reactive oxygen content in H_2O_2 (47.1 % w/w) is the highest among all chemicals. No toxic by-products are produced from H_2O_2, making H_2O_2 a highly efficient and environmental-friendly oxidant. H_2O_2 has been widely applied for disinfection and sterilization (McDonnell G., 2014; Teng Z. et al., 2019), organic synthesis (Zhan W. et al., 2018) and wastewater treatment (Zhang M.-h. et al., 2019). A one-compartment fuel cell using H_2O_2 in which H_2O_2 is used as both an oxidant and a reductant has recently been developed (Mousavi Shaegh S.A. et al., 2012). Studies on this fuel cell showed that the theoretical output potential is 1.09 V, which is comparable to that of a conventional hydrogen (H_2) fuel cell (1.23 V) (Mousavi Shaegh S.A. et al., 2012; Kim D. et al., 2015; Yamada Y. et al., 2013). Compared to H_2, H_2O_2 showed a promising prospect as a water-soluble solar fuel (H_2O_2, 3.0 MJL^{-1}, in an aqueous solution higher than the intensity of compressed H_2 gas, 2.8 MJL^{-1}, 35 MPa) (Kim D. et al., 2015). Unlike hydrogen, H_2O_2 is fully soluble in water and is easily transportable, making it an ideal energy carrier alternative to H_2. The anthraquinone (AQ) method for H_2O_2 production is the main process used in industry (more than 95 % of total production, **Fig. 1**) (Campos-Martin J.M. et al., 2006). The AQ process includes the following four steps: (i) in an organic solvent, hydrogenation of anthraquinone (AQ) is firstly catalyzed on an Ni/Pd catalyst; (ii) hydrogenated anthraquinone (HAQ) is oxidized with the aid of a catalyst; (iii) H_2O_2 is extracted by pure water, and HAQ is used to reproduce AQ; and iv) the as-prepared H_2O_2 is purified and concentrated for following commercial use. These hydrogenation and oxidation reactions consume a lot of energy. Additionally, the AQ process is not environmental-friendly because large amounts of wastes are generated (Campos-Martin J.M. et al., 2006).

Efforts have been made to develop new methods for H_2O_2 production under more moderated reaction conditions with less waste production. (Yi Y. et al., 2016). Direct synthesis from H_2 and O_2 in the presence of a Pd catalyst or a bimetallic Au–Pd catalyst is a possible alternative route for H_2O_2 production based on the reaction of $H_2 + O_2 = H_2O_2$. Typical reaction conditions mainly include H_2/O_2 mixture gas catalyzed by noble metal catalysts (Xia C. et al., 2019; Freakley S.J. et al., 2016). The ratio of the H_2/O_2 mixture needs to be precisely controlled in the process to avoid the risk of explosions (Xia C. et al., 2019; Freakley S.J. et al.,

† Received 22 December 2021; Accepted 6 February 2022
J-STAGE Advance published online 2 April 2022
Add: 1-1 Sensuicho, Tobata Ward, Kitakyushu, Fukuoka 804-8550, Japan
E-mail: tohno@che.kyutech.ac.jp
TEL: +81-093-884-3318 FAX: +81-72-867-1658

Copyright © 2023 The Authors. Published by Hosokawa Powder Technology Foundation. This is an open access article under the CC BY license (https://creativecommons.org/licenses/by/4.0/).

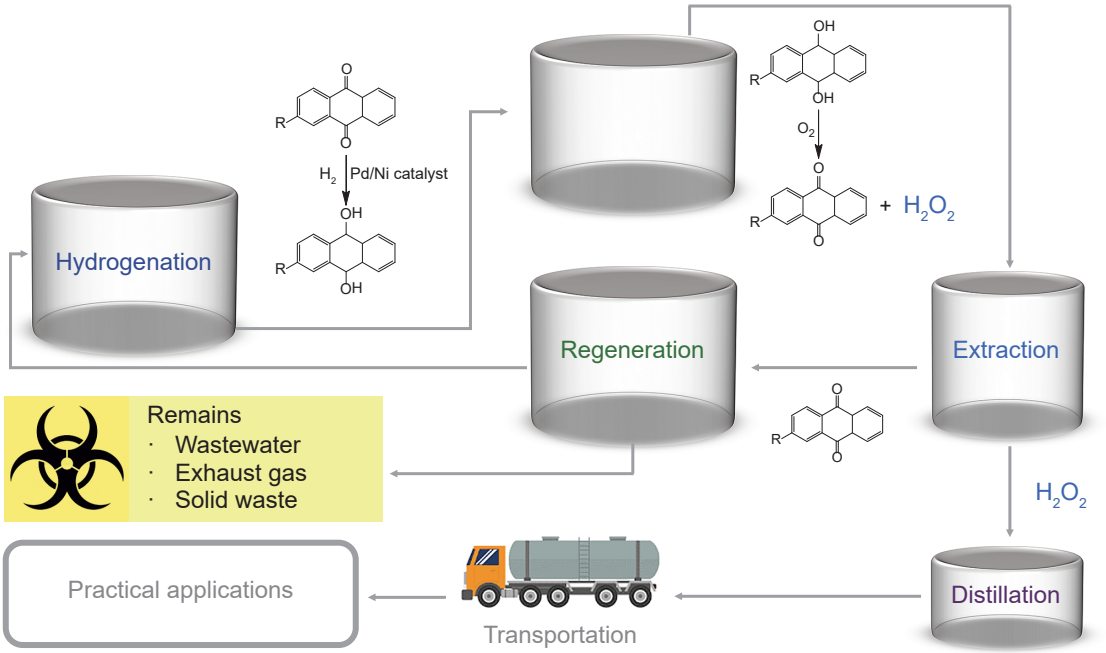

Fig. 1 Schematic of the anthraquinone oxidation (AQ) process.

2016). Recently, much attention has been given to the possibility of efficient H_2O_2 production by a photocatalytic reaction process, which would be a significant breakthrough in H_2O_2 chemistry. A photocatalytic approach would enable the use of explosive H_2 gas to be avoided and it would only need light, O_2 and water, with no pollutant generated in the overall process. Much interest has therefore been shown in photocatalytic strategies for H_2O_2 production.

In past one decade, many kinds of semiconductors including metal oxides, metal sulfides, metal organic compounds and organic semiconductors have been prepared for photocatalytic H_2O_2 production (Hou H. et al., 2020). Among these photocatalysts, graphite-like carbon nitride (g-C_3N_4), also named polymeric carbon nitride (PCN), as a metal-free polymer semiconductor (n-type), possesses a stacked two-dimensional (2D) structure of tri-*s*-triazine connected via tertiary amines (Wang X. et al., 2009). Because of its unique electrical, optical, structural and physicochemical properties, g-C_3N_4 has been recognized as a new class of cost-efficient multifunctional materials for electronic, catalytic and energy applications (Banerjee T. et al., 2021). Shiraishi and co-workers first found in 2014 that pristine g-C_3N_4 showed some photocatalytic activity for H_2O_2 production with the addition of ethanol as an electron donor (Shiraishi Y. et al., 2014b). Since then, more than 80 studies on photocatalytic H_2O_2 production based on g-C_3N_4 materials have been published. Several reviews summarizing some of the recent progress in photocatalytic H_2O_2 production have also been published (Hou H. et al., 2020; Zhang G. et al., 2020). Most of those reviews focused on how the various protocols for preparation of functionalized g-C_3N_4 influenced the photocatalytic activity (Hou H. et al., 2020; Zhang G. et al., 2020). However, it is difficult to reveal the inner relationships among the structure, properties and performance of a g-C_3N_4-based photocatalyst by simply summarizing preparation methods, properties and performances (Zhang G. et al., 2020; Torres-Pinto A. et al., 2019). Generally, the structure of a photocatalyst defines its properties, and the properties of the photocatalyst determine its performance. Thus, it is necessary to determine the desired properties of a g-C_3N_4-based photocatalyst for H_2O_2 production. Determination of the desired properties would lead to a comprehensive understanding of the photocatalyst from rational structure design to good performance.

In this review, we firstly show the principles of photocatalytic H_2O_2 production. Then the three most important issues for improving H_2O_2 generation based on the band diagram and physicochemical properties of pristine g-C_3N_4 are proposed. By combining the fundamental principles with preparation strategies and possible influencing factors in liquid-phase photocatalytic systems, future challenges and possible directions for H_2O_2 production using functionalized g-C_3N_4 catalysts are presented in this review with the hope that they will inspire design and preparation strategies for not only carbon nitrides but also a variety of photocatalysts with good performance.

2. Principles of photocatalytic H_2O_2 generation

Since solar energy is renewable and sustainable, photocatalysis using power systems has received much attention in the past few years and it has been applied to various fields including water splitting for H_2 and O_2 production

(Wang X. et al., 2009; Wang Q. and Domen K., 2020), CO_2 reduction (Liu R. et al., 2020), nitrogen fixation (Zhang G. et al., 2020), degradation of pollutants (Koe W.S. et al., 2020) and disinfections (Teng Z. et al., 2019), organic synthesis and H_2O_2 production (Hou H. et al., 2020). Photocatalytic power systems are cost-efficient and easy to operate compared with photo-electrochemical systems and photovoltaic-electrochemical systems (Hisatomi T. and Domen K., 2019). There are three typical steps in a photocatalytic process (**Fig. 2**) (Nosaka Y. and Nosaka A., 2016). Sufficient light absorption, efficient charge separation, and surface reactions are crucial properties for typical efficient photocatalysts.

Photocatalytic production of H_2O_2 follows the photocatalytic reaction principles. H_2O_2 can be generated through either oxygen reduction reaction (ORR) or water oxidation reaction (WOR) (Fan W. et al., 2020) as shown by a schematic diagram of photocatalytic H_2O_2 production in **Fig. 3**. The light-driven $2e^-$ WOR pathway (Eqn. (3), **Table 1**) is difficult to be achieved because of the uphill thermodynamics (1.76 V vs. a reversible hydrogen electrode, simplified as RHE, **Table 1**), i.e., the decomposition of as-produced H_2O_2 will occur at this potential (1.76 V) because H_2O_2 is an excellent hole scavenger (Shi X. et al., 2017). In the case of the ORR pathway, H_2O_2 can be produced by either a $2e^-$ direct oxygen reduction ($O_2 \rightarrow H_2O_2$) route or a sequential $1e^-$ indirect reduction ($O_2 \rightarrow {\bullet}O_2^- \rightarrow H_2O_2$). For h^+ in consumption, the most effective reaction route is to oxidize H_2O into O_2 and H^+ via a $4e^-$ pathway (Eqn. (1)). Eqn. (7) to Eqn. (10) in **Table 1** show production of H_2O_2 via the two-step $1e^-$ reduction pathway. First, superoxide radicals ($\bullet O_2^-$) are formed (Eqn. (7)) and further produce $HO_2\bullet$ radicals with the reaction of H^+ (Eqn. (8)). Then, the $HO_2\bullet$ radicals could produce HO_2^- anions by undergoing another $1e^-$ reduction (Eqn. (9)). Finally, HO_2^- reacts with H^+ to generate H_2O_2. Eqn. (2) shows the one-step $2e^-$ direct reduction for H_2O_2 production. In this process, O_2 directly reacts with two protons to form an H_2O_2 product via two-electron photoreduction. It should be noted that the back reaction of WOR via a $4e^-$ pathway is the ORR process via a $4e^-$ pathway (Eqn. (1)), which could also be a competitive reaction for H_2O_2 production via $2e^-$ ORR. The most ideal situation would be for photocatalytic production of H_2O_2 to be generated from H_2O and O_2 via $4e^-$ WOR and $2e^-$ ORR, which is an uphill reaction ($\Delta G_0 = 117$ kJ mol^{-1}).

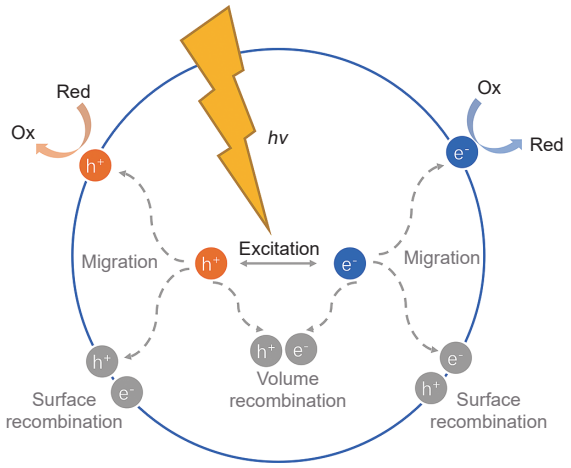

Fig. 2 Photoexcitation and charge decay pathway.

3. Desired physicochemical properties of polymetric carbon nitride for photocatalytic H_2O_2 production

Since Wang and his co-workers first discovered the photocatalytic activities of g-C_3N_4 (Wang X. et al., 2009), g-C_3N_4-based particulate photocatalysts have attracted much interest. The band gap of g-C_3N_4 (Carbon nitrides produced by thermal treatment at 500~550 °C with nitrogen-rich precursors have various names as polymeric carbon nitride (PCN), graphitic carbon nitride (GCN), and melon) is ~2.7 eV, corresponding to an optical wavelength of ~460 nm, which makes it a promising visible-light-response photocatalyst with an appropriate band structure (**Fig. 4**) (Ong W.-J. et al., 2016; Hou H. et al., 2020). Additionally, the conjugated heptazine ring in the PCN matrix can provide active sites for $2e^-$ ORR (Shiraishi Y.

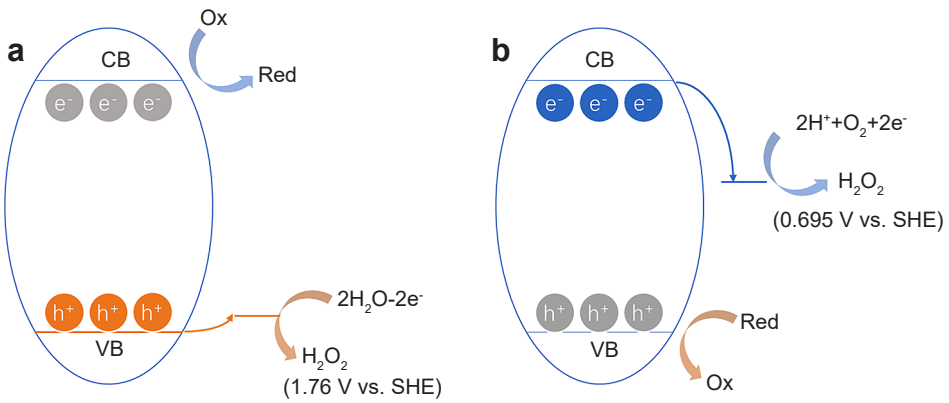

Fig. 3 Schematic diagram for photocatalytic H_2O_2 production. **(a)** Photocatalytic H_2O_2 production via water oxidation reaction. **(b)** Photocatalytic H_2O_2 production via oxygen reduction. CB is the abbreviation for conduction band. VB is the abbreviation for valence band.

Table 1 Standard electrode potentials for aqueous ORR half-reactions (Gao J. and Liu B., 2020). Reprinted with permission from Ref. (Gao J. and Liu B., 2020). Copyright: (2020) American Chemical Society.

Eqn. No.	Half-reactions	E^0 (V vs. SHE*)	E^0 (V vs. RHE**)
(1)	$O_2(g) + 4H^+ + 4e^- \leftrightarrow 2H_2O$	1.229	1.229
(2)	$O_2(g) + 2H^+ + 2e^- \leftrightarrow H_2O_2$	0.695	0.695
(3)	$H_2O_2 + 2H^+ + 2e^- \leftrightarrow 2H_2O$	1.763	1.763
(4)	$O_2(g) + 2H_2O + 4e^- \leftrightarrow 4OH^-$	0.401	1.229
(5)	$O_2 + H_2O + 2e^- \leftrightarrow HO_2^- + OH^-$	–0.065	0.764
(6)	$HO_2^- + H_2O + 2e^- \leftrightarrow 3OH^-$	0.867	1.696
(7)	$O_2(g) + e^- \leftrightarrow O_2^-$	–0.33	–0.33
(8)	$O_2(g) + H^+ + e^- \leftrightarrow HO_2\bullet$	–0.05	–0.05
(9)	$HO_2\bullet + e^- \leftrightarrow HO_2^-$	0.76	0.76
(10)	$HO_2\bullet + H^+ + e^- \leftrightarrow H_2O_2$	1.44	1.44
(11)	$H_2O_2 + H^+ + e^- \leftrightarrow H_2O + \bullet OH$	0.793	0.793
(12)	$\bullet OH + e^- \leftrightarrow OH^-$	1.89	2.72

*SHE: Standard hydrogen electrode.
**RHE: Reversible hydrogen electrode.

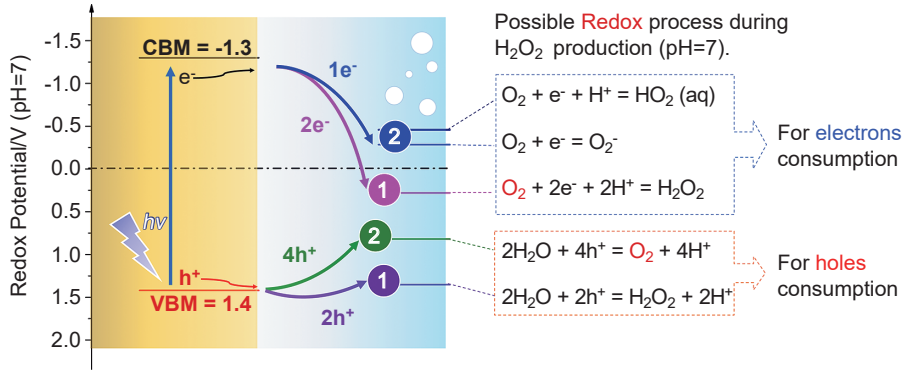

Fig. 4 Band diagrams of g-C_3N_4 and summary of potentials for redox reactions during H_2O_2 production by using O_2 and/or H_2O. CBM is the abbreviation for conduction band minimum and VBM is the abbreviation for valence band maximum.

et al., 2014a; Shiraishi Y. et al., 2014b), which is similar to the catalytic properties of graphene for 2e⁻ ORR (Kim H.W. et al., 2018; Lu Z. et al., 2018). As such, g-C_3N_4 has emerged as a star material in the field of photocatalytic H_2O_2 production.

However, the activity of g-C_3N_4 for photocatalytic H_2O_2 production is still restricted by low efficiency because of some drawbacks of pristine g-C_3N_4. Firstly, a large concentration of defects is inevitably introduced into g-C_3N_4 during thermal polymerization (Kim D. et al., 2015; Ong W.-J. et al., 2016). This means that the inner-plane structure of g-C_3N_4 is not completely composed of covalent bonds, i.e., the interactions are hydrogen bonds between melons ($[C_6N_9H_3]_n$) (**Fig. 5**) (Kessler F.K. et al., 2017). As a result, the charge separation and charge migration are significantly hindered, resulting in a high charge recombination rate of PCN. Secondly, the large band gap (2.7 eV) and small absorption of visible light (Kubelka-Munk absorbance usually less than 2, $\lambda = 420$ nm) result in insufficient visible-light harvesting. Thirdly, although the side-on adsorption of molecular oxygen on the π-conjugated heptazine ring enables g-C_3N_4 (Shiraishi Y. et al., 2014b) to have some selectivity for 2e⁻ ORR, it is difficult for the stepwise 1e⁻ to 1e⁻ ORR reaction to be prevented since signals of superoxide radicals can still be detected during the photocatalytic reactions with electron spin resonance during the photocatalytic reactions (Li S. et al., 2016). In this case, reaction sites with higher selectivity for 2e⁻ ORR have to be constructed for improving the overall activity. To overcome these drawbacks, many protocols including tuning morphologies, defect engineering, loading co-catalysts, copolymerization of semiconductors, doping elements and hybridization have been developed. Each of these functionalization strategies overcome one or two

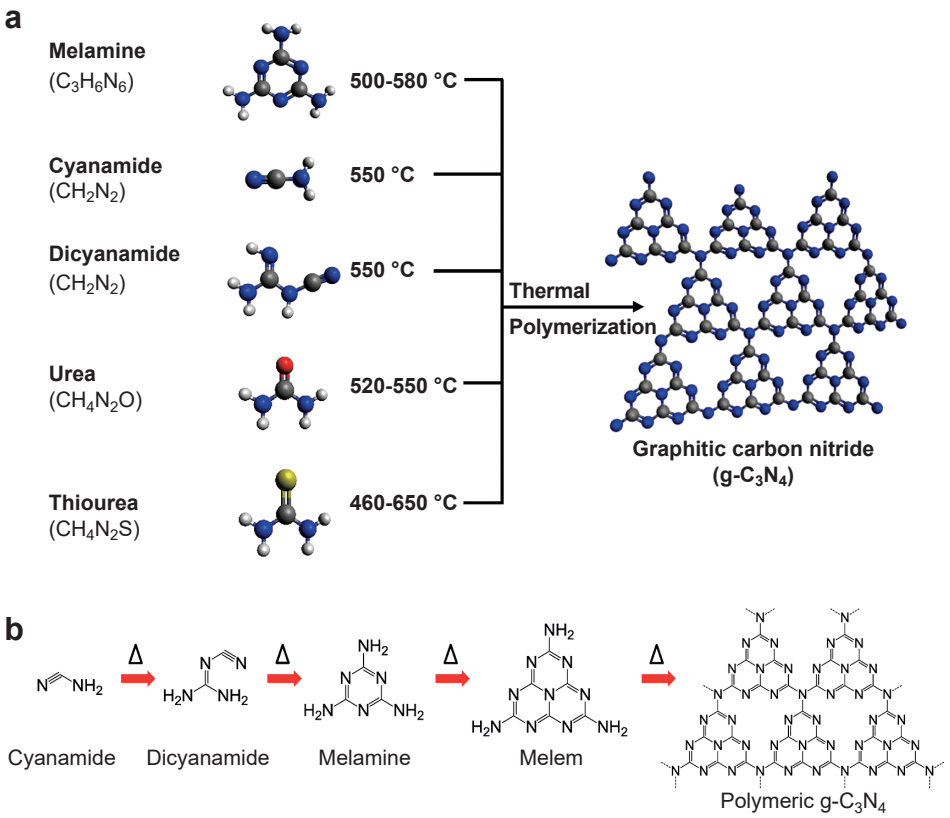

Fig. 5 **(a)** Schematic illustration of the synthesis process of g-C_3N_4 by thermal polymerization of different precursors such as melamine, cyanamide, dicyanamide, urea, and thiourea. The black, blue, white, red, and yellow balls denote C, N, H, O, and S atoms, respectively. **(b)** Reaction pathway for the development of g-C_3N_4 using cyanamide as the precursor. Reprinted with permission from Ref. (Ong W.-J. et al., 2016). Copyright: (2016) American Chemical Society.

drawbacks by changing the following properties of pristine PCN: (i) suppressing charge recombination, (ii) narrowing the bandgap or/and promoting light absorbance, and (iii) introducing active sites for selective 2e⁻ ORR (**Fig. 6**). Based on the improved physicochemical properties, functionalization strategies for improvement in the activity for photocatalytic H_2O_2 production can also be divided into three parts, which provide a comprehensive understanding from material preparation to physicochemical properties, thus providing the insight into the relationships among structure, properties and performance.

3.1 Suppressing charge recombination

3.1.1 Hybridization

3.1.1.1 Hybridization with carbon-based materials

Carbonaceous nanomaterials are promising modifiers for photocatalysts because of their sp^2-hybridized electronic structures (Shiraishi Y. et al., 2014a; Kim H.W. et al., 2018; Lu Z. et al., 2018; Yang S. et al., 2018). These materials usually work as electron transfer materials and photosensitizers to broaden the adsorption edge and improve the charge migration (Yang S. et al., 2018; Thakur S. et al., 2017; Zeng X. et al., 2017).

Carbon nanotubes (CNTs) with a π-conjugative structure are capable of accepting, transporting and storing electrons for g-C_3N_4 (Tasis D. et al., 2006). An amination reaction process was developed by Zhao and co-workers to introduce CNTs into nanosheets of g-C_3N_4, in which g-C_3N_4 was covalently combined with CNTs (**Fig. 7a**, **b**) (Zhao S. et al., 2018a). The CNTs covalently combined with g-C_3N_4 promoted charge migration by shifting the CB level to enhance the single-electron reduction of O_2 to $\cdot O_2^-$, thus leading to enhanced ORR activity (Zhao S. et al., 2018a). As shown in **Fig. 7c**, the photocurrent of g-C_3N_4/CNTs was significantly increased compared with that pristine PCN. Shiraishi and co-workers also used reduced graphene oxide (rGO) for hybridization with a g-C_3N_4/perylene diimide (PDI) catalyst for further activity improvement (**Fig. 7d, e**). The improved activity may due to the ultra-thin two-dimensional nature of rGO (g-C_3N_4/PDI/$rGO_{0.05}$) with high charge carrier mobility (Kofuji Y. et al., 2016a). As shown in **Fig. 7f**, the photocurrent of g-C_3N_4/PDI/$rGO_{0.05}$ is significantly larger than that of g-C_3N_4/PDI. However, no current response is found by using a rGO electrode, indicating a synergic effect of g-C_3N_4/PDI and rGO. It should be noted that the formation of tight junctions between the g-C_3N_4-based photocatalyst and carbon-based material is extremely important for the formation of electron transfer pathways since the photocurrent intensity of the physical mixture of rGO and g-C_3N_4/PDI is 20 % smaller than

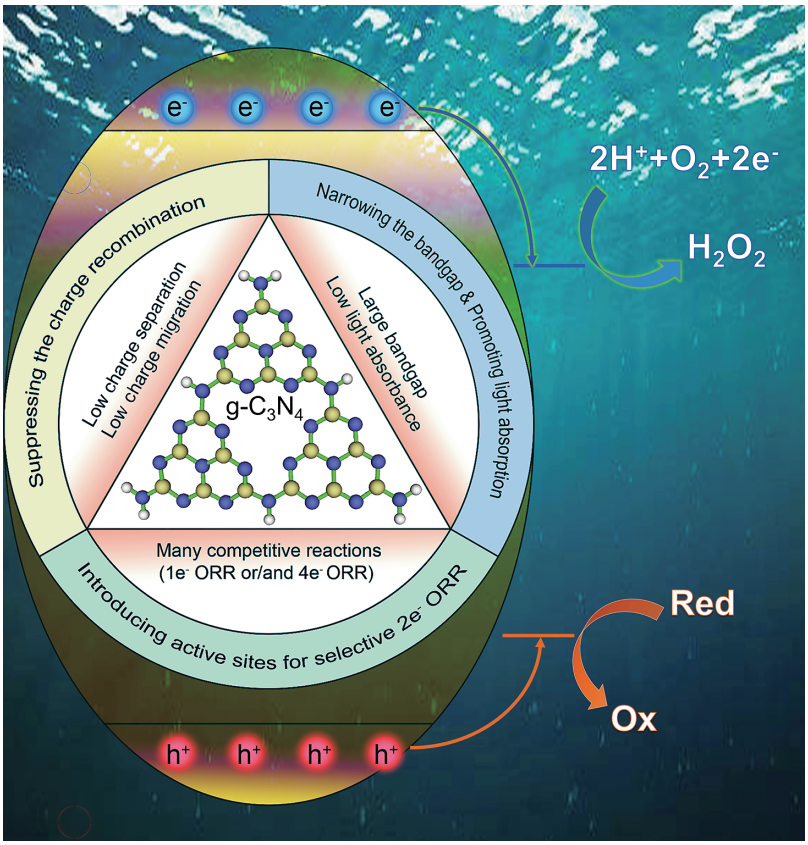

Fig. 6 Solutions for overcoming the disadvantages of pristine g-C_3N_4 by manipulating physicochemical properties via $2e^-$ ORR.

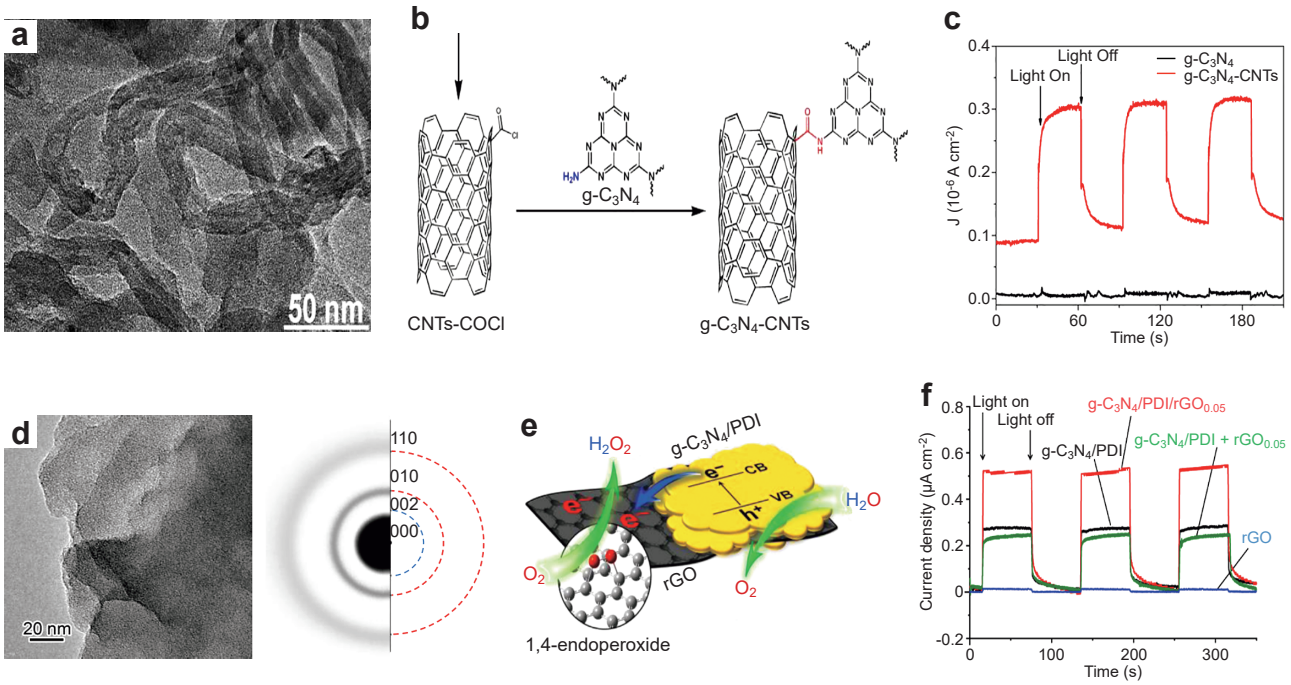

Fig. 7 Hybridization with a carbon-based material for improved charge separation. **(a)** TEM images of g-C_3N_4-CNTs. **(b)** Process for preparation of g-C_3N_4-CNTs. **(c)** Photocurrent response of g-C_3N_4-CNTs or g-C_3N_4-loaded electrodes under light at a bias of 0.25 V vs. SCE ($\lambda \geq 400$ nm). **(d)** TEM image of g-C_3N_4/PDI/r$GO_{0.05}$ and its SAED pattern (inverse contrast) with indexed graphite pattern. **(e)** Schematic illustration of the proposed mechanism for photocatalytic H_2O_2 production on g-C_3N_4/PDI/rGO. **(f)** Photocurrent responses of g-C_3N_4/PDI/r$GO_{0.05}$ and other g-C_3N_4-based catalysts measured on FTO in 0.1 M Na_2SO_4 solution under visible light ($\lambda > 420$ nm) at a bias of 0.5 V (vs Ag/AgCl). SCE is an abbreviation for saturated calomel electrode, SAED is an abbreviation for selected area electron diffraction, and FTO is an abbreviation for fluorine-doped tin oxide. Reprinted with permission from Ref. (Zhao S. et al., 2018a; Kofuji Y. et al., 2016a). Copyright: (2018) Elsevier and (2016) American Chemical Society.

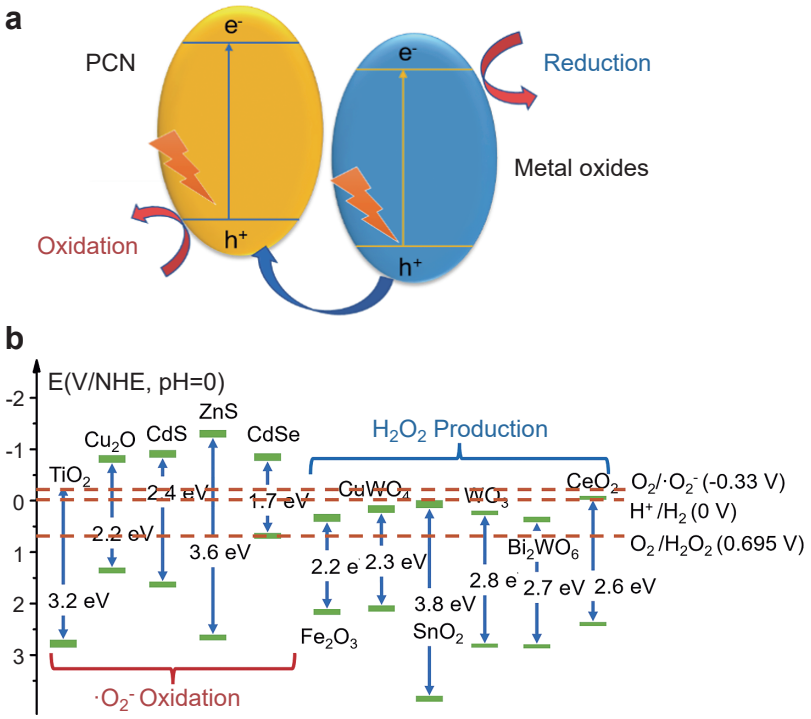

Fig. 8 Schematic diagram of **(a)** semiconductor heterojunctions and **(b)** diagram of band positions based on experimental results for common metal-based photocatalysts. NHE is an abbreviation for normal hydrogen electrode.

the photocurrent density of g-C_3N_4/PDI (Kofuji Y. et al., 2016a).

3.1.1.2 Hybridization with metal and metal compounds

Fabrication of metal compounds to form a Schottky barrier between metal-based semiconductors and PCN material has been proved to be an efficient approach for enhancing the photocatalytic efficiency for several reactions (Ong W.-J. et al., 2016; Teixeira I.F. et al., 2018). The nature of the formation of Schottky barriers in PCN/metal compounds is due to the differences between the charge potentials of metal compounds and PCN under light irradiation (Zhang Z. and Yates J.T., 2012). The electrons tend to migrate to semiconductors that have more positive potentials, while holes tend to migrate to those with negative potentials (Nosaka Y. and Nosaka A., 2016). Although the overall redox potential of the photocatalyst is decreased, the charge separation of charge carriers is significantly improved, thus leading to a significantly improved charge separation (**Fig. 8a**). However, there are very few reports on the promotion of photocatalytic efficiency for H_2O_2 production by construction of heterojunctions based on PCN/metal compounds. There are two possible reasons. On the one hand, the potential of the conduction band minimum (0.9~1.3 V vs. SHE) of PCN (**Fig. 4**) is more negative than that of common metal compounds. In this case, the photoelectrons tend to accumulate on the metal oxides. Thus, the potential of the metal compounds determines the reduction potential of the heterojunction materials. As shown in **Fig. 8b**, the photocatalytic reduction potential of TiO_2, Cu_2O, CdS and ZnS can hardly facilitate $2e^-$ ORR because of the kinetically favored $1e^-$ ORR to form $\bullet O_2^-$, thus resulting in a stepwise ORR to generate H_2O_2. For other metal compound semiconductors, $1e^-$ ORR can be prevented because of the positively shifted CBM. However, the potential differences between the redox potentials of O_2, $2H^+/H_2O_2$ and CBM of Fe_2O_3, $CuWO_4$, SnO_2, WO_3, etc. are quite small, which may lead to a poor thermodynamic driving force for $2e^-$ ORR. On the other hand, formed H_2O_2 can be decomposed by metal compounds by disproportionation or photoreaction (Li X. et al., 2001). Therefore, the formation of heterojunctions by contact of PCN with one metal compound may be an unacceptable strategy unless a unique electron transfer pathway between PCN and metal compounds is formed, such as in Z-scheme catalysts, so that reduction will occur on the surface of PCN (Wang S. et al., 2020a).

Loading active noble metal nanoparticles (NPs) is one of the effective approaches for boosting the photocatalytic activity of a photocatalyst for H_2O_2 production (Hirakawa H. et al., 2016; Tsukamoto D. et al., 2012). Zuo and coworkers observed a similar improvement in the activity of an Au/C_3N_4 photocatalyst for H_2O_2 production (Zuo G. et al., 2019). In that study, the effects of different noble-metal cocatalysts on g-C_3N_4 for H_2O_2 production were also compared, and the results showed that g-C_3N_4 loaded with Au nanoparticles (NPs) had the highest activity for H_2O_2

production (Zuo G. et al., 2019). The enhancement of H_2O_2 production was attributed to the efficient separation of photogenerated electrons and holes between Au NPs and g-C_3N_4 (Zuo G. et al., 2019). The function of Au NPs on PCN for charge separation is similar to that of carbon materials. The Au NPs can improve the carrier mobility of photoelectrons so that the charge recombination can be suppressed.

3.1.1.3 Hybridization with metal-free semiconductors and molecules

The advantages of cost efficiency, mechanical flexibility and easy operation makes organic semiconductors promising alternatives for inorganic materials to improve the charge separation (Chung D.D.L., 2019). Triazine (Jiang X. et al., 2015) and aromatic diimides have been used as modifiers for g-C_3N_4 based photocatalysts (Shiraishi Y. et al., 2014a; Kofuji Y. et al., 2016a; Kofuji Y. et al., 2018; Kofuji Y. et al., 2017; Kofuji Y. et al., 2016b). Shiraishi and co-workers incorporated several aromatic diimides (Shiraishi Y. et al., 2014a; Kofuji Y. et al., 2018; Kofuji Y. et al., 2016b; Kofuji Y. et al., 2017) into the g-C_3N_4 matrix by thermal condensation (**Fig. 9a**). All of the g-C_3N_4/PDI, g-C_3N_4/biphenyl diimide (BDI) and g-C_3N_4/mellitic triimide (MTI) catalysts successfully produced H_2O_2 (millimolar level) in pure water with O_2 (Shiraishi Y. et al., 2014a; Kofuji Y. et al., 2016a; Kofuji Y. et al., 2018; Kofuji Y. et al., 2017; Kofuji Y. et al., 2016b). The photocurrent showed a significant improvement after the copolymerization of aromatic diimides. It should be noted that the introduction of more C=O groups significantly improved the photocurrent (**Fig. 9b**) (Kofuji Y. et al., 2017). The C=O groups in these aromatic diimides may accumulate negative charges and then increase the thickness of the space-charge region, which might improve the separation efficiency of charge carriers (Koe W.S. et al., 2020) and disinfections (Teng Z. et al., 2019). Based on this phenomenal result from the properties of C=O groups, Ohno and co-workers prepared C=O functionalized PCN by copolymerization of 2,5,8-triamino-tri-*s*-triazine (melem) and barbituric acid (BA) (PCNBA, **Fig. 9c**) (Teng Z. et al., 2020). In the photoluminescence (PL) spectra (**Fig. 9d**), there was a significant decrease in intensity together with a notable increase in photocurrent intensity (Teng Z. et al., 2020). The copolymerization of BA significantly suppressed recombination and accelerated the charge separation.

In the case of incorporation with semiconductors, Shiraishi and co-workers combined PCN/PDI with boron nitride (BN) to separate holes since BN has a relatively negative VBM (Kofuji Y. et al., 2018). In the system of g-C_3N_4-PDI-$BN_{0.2}$-rGO, the photocurrent increased about 20 % (Kofuji Y. et al., 2018). It is notable that the oxygen evolution of g-C_3N_4-PDI-$BN_{0.2}$-rGO was increased by more than 15 % compared with that of g-C_3N_4-PDI-rGO (Kofuji Y. et al., 2016a), further confirming that the charge separation introduced by BN separated photogenerated holes, leading to

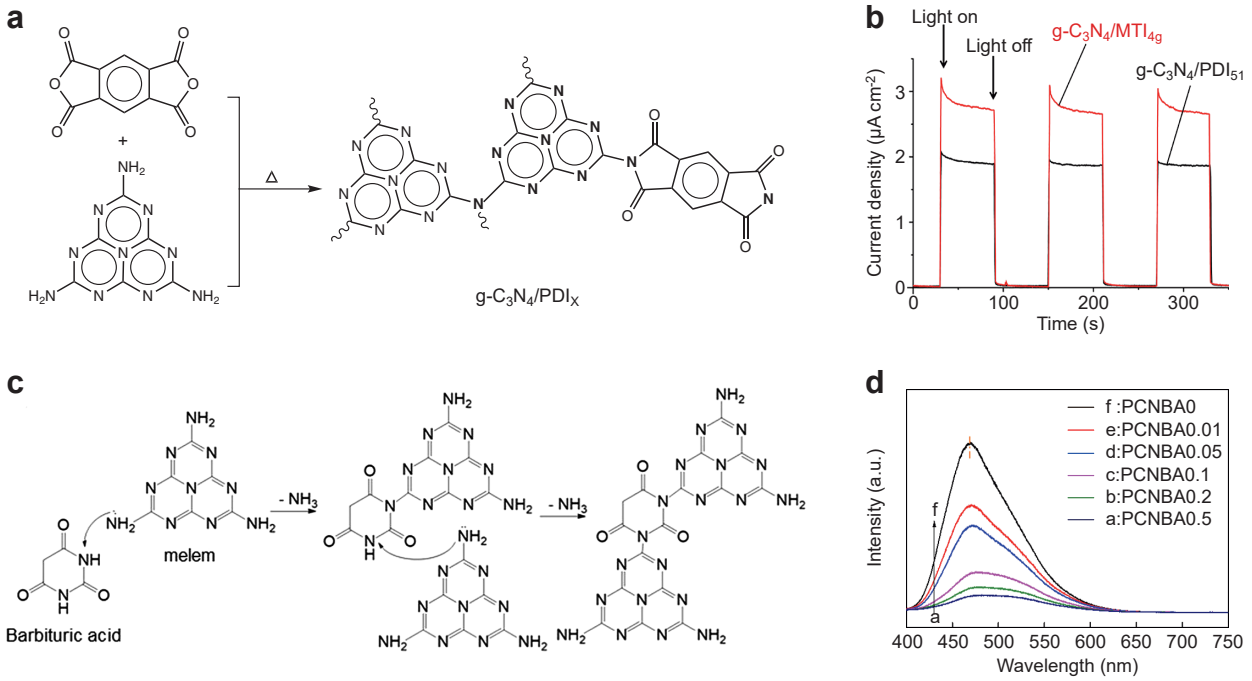

Fig. 9 Hybridization with electron-deficient organic semiconductors for improved charge separation. **(a)** Scheme of the synthesis of g-C_3N_4 hybridized by aromatic diimide using g-C_3N_4/PDI_x as an example. **(b)** Photocurrent responses of g-C_3N_4/MTI_{49} and g-C_3N_4/PDI_{51} in 0.1 M Na_2SO_4 (bias: 0.5 V vs Ag/AgCl). **(c)** Process for polymerization of PCNBA with barbituric acid and melem as precursors. **(d)** Photoluminescence spectra of PCN and PCNBA samples. Reprinted with permission from Ref. (Kofuji Y. et al., 2017; Teng Z. et al., 2020). Copyright: (2017) American Chemical Society and (2020) Elsevier.

an improved charge separation. Perylene imides (PIs) were modified on g-C_3N_4 nanosheets (Yang L. et al., 2017) to fabricate a Z-scheme configuration for promotion of charge separation. As a result, more electrons from the CB of the g-C_3N_4 part efficiently generated H_2O_2, while the holes of g-C_3N_4/PI oxidized OH^- to OH (Yang L. et al., 2017), which also subsequently reacted to produce H_2O_2.

3.1.2 Doping

3.1.2.1 Metal and non-metal doping

Optical, electronic and other physical properties of g-C_3N_4 materials could be manipulated by doping strategies that introduce additional elements and impurities into the framework (Liu X. et al., 2020). In the case of charge separation, one of the most efficient strategies is to incorporate alkaline metal ions. Alkaline metal ions were used in several works to functionalize PCN, leading to a promoted charge separation for organic synthesis (Qiu C. et al., 2018) (**Fig. 10a**). Hydrogen evolution reduction (HER) (Sun S. et al., 2019), carbon dioxide reduction (COR) (Wang S. et al., 2020b), and nitrogen fixation, (Li X. et al., 2018a) can all be facilitated by incorporation of alkaline metal ions into PCN. Moon and co-workers incorporated potassium (K), phosphorus (P), and oxygen (O) elements into a g-C_3N_4 matrix by thermal calcination of melamine with potassium phosphate (KPD, K_2HPO_4) (Moon G.-h. et al., 2017). The charge separation of KPD was significantly improved because of the significantly decreased PL intensity (**Fig. 10b**). The hector-elements in the g-C_3N_4 matrix increased the carrier lifetime to a picosecond range. Consequently, the generation rate of H_2O_2 by K-P-O-doped g-C_3N_4 was notably promoted compared to that by pure g-C_3N_4 (Moon G.-h. et al., 2017) (**Fig. 10c**). Halogen (Br or Cl)-doped g-C_3N_4 nanorods could also accelerate H_2O_2 production (Zhang C. et al., 2018). The charge carrier transfer in the matrix of g-C_3N_4 was promoted by the introduction of heteroatoms (Zhang C. et al., 2018). Kim et al. studied the co-doping of metal (K) and nonmetal ions (P and F) into the g-C_3N_4 framework (Kim S. et al., 2018). The co-doped g-C_3N_4 also significantly promoted charge separation. Under visible light irradiation, the co-doped g-C_3N_4 exhibited higher activity for photocatalytic production of H_2O_2 than that of bare g-C_3N_4 (**Fig. 10d**).

Zhang et al. used density functional theory (DFT) calculation to reveal how the incorporated alkaline ions change the charge distribution over different atoms (Zhang

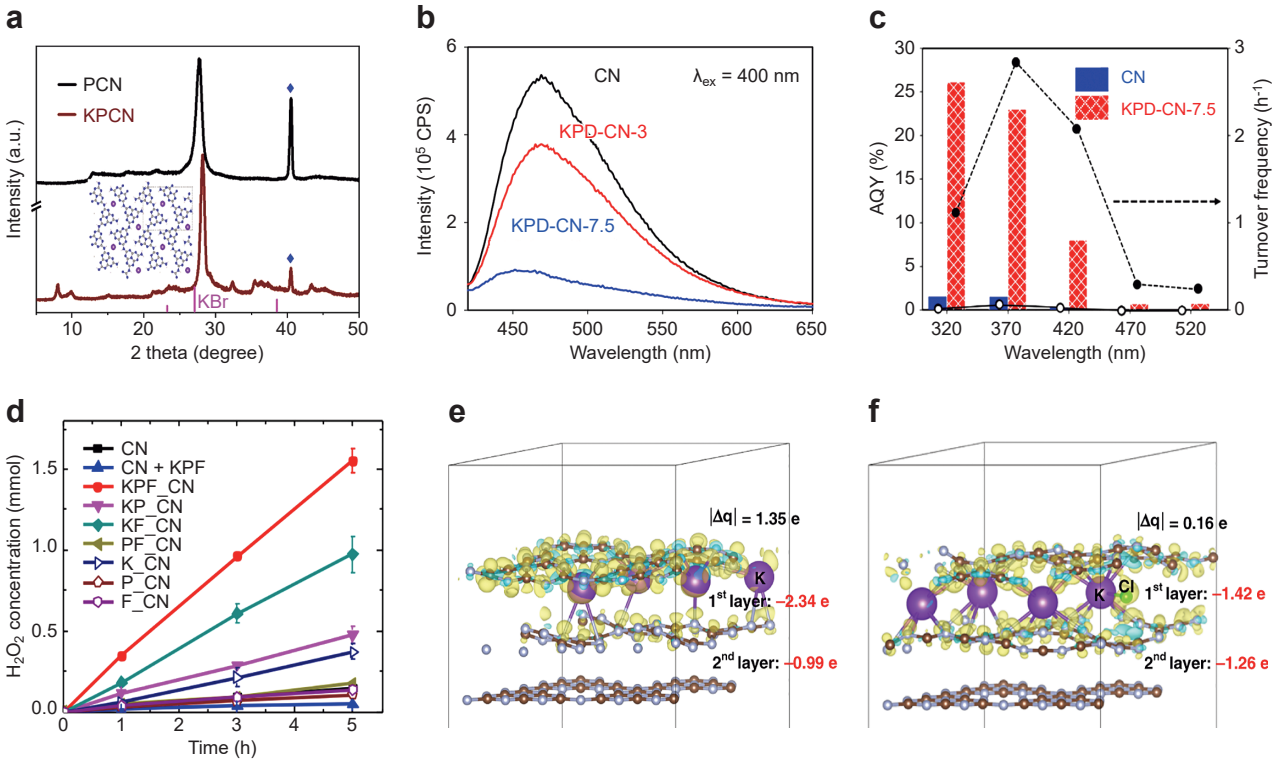

Fig. 10 Metal and/or non-metal doping for improving the charge separation. **(a)** XRD patterns of pristine PCN and K^+-incorporated PCN. **(b)** PL emission spectra (λ = 400 nm) of bare carbon nitride (CN), KPD-CN-3, and KPD-CN-7.5. **(c)** Apparent quantum yield (AQY, left axis) and turnover frequency (right axis) of bare CN and those of KPD-CN-7.5 for H_2O_2 production with monochromatic light irradiation. **(d)** Time profiles of photocatalytic H_2O_2 generation using CN samples modified with various dopants and a control sample of a physical mixture of CN and KPF_6 (CN + KPF). The experimental conditions were 0.5 g L^{-1} photocatalyst, 10 vol% ethanol, pH 3, continuously purged with O_2 and polychromatic light through a long pass filter (k > 420 nm). Charge distributions of **(e)** K-GCN and **(f)** KCl-GCN obtained from density functional theory (DFT) calculations. Reprinted with permission from Ref. (Qiu C. et al., 2018; Moon G.-h. et al., 2017; Kim S. et al., 2018; Zhang P. et al., 2019). Copyright: (2018) The Authors (Qiu C. et al.), published by John Wiley & Sons, (2017) American Chemical Society, (2018) Elsevier and (2019) Springer Nature Ltd.

P. et al., 2019). The introduction of incorporated potassium species resulted in an accumulation on the first PCN layer. With the further assistance of Cl atoms, the electron distribution between the layers was more balanced (**Fig. 10e** and **10f**), thus leading to a significantly improved interlayer charge transfer (Zhang P. et al., 2019).

Non-metal doping of PCN also enables manipulation of the electronic configuration of PCN with significantly improved charge separation (Zhang P. et al., 2020). Wei et al. developed an oxygen-enriched g-C_3N_4 (OCN) photocatalyst that achieved enhanced H_2O_2 production (Wei Z. et al., 2018). Compared to g-C_3N_4, the OCN samples achieved significantly enhanced no-sacrificial H_2O_2 production efficiency. Electrochemical impedance spectroscopy (EIS) and photoluminescence (PL) spectra all proved that charge separation efficiency was significantly promoted after the O element had been introduced into the PCN matrix.

3.1.2.2 Doping with polyoxometalates and their derivatives

Polyoxometalates (POMs) are composed of cations and polyanion clusters with high structural diversity (Han X.-B. et al., 2015). Under light irradiation, a charge transfer from O^{2-} to M^{n+} (n = 5, 6) usually occurred in these catalysts and lead to the formation of a hole center (O^-) and trapped electron center ($M^{(n-1)+}$) pair. POMs in the PCN matrix can serve as electron donor-acceptor pairs, which could significantly promote the charge separation or/and serve as co-catalysts (Han X.-B. et al., 2015). Zhao and coworkers synthesized a series of POMs clusters-modified g-C_3N_4 samples for efficient photocatalytic H_2O_2 evolution by the thermal condemnation method (Zhao S. et al., 2017; Zhao S. and Zhao X., 2019; Zhao S. et al., 2018b). The amount of H_2O_2 formed by g-C_3N_4/PW_{11} reached 3.5 μmol within 60 min, while the catalytic performance of pure g-C_3N_4 was only 1.3 μmol (Zhao S. et al., 2017). That research group also used other POM clusters, including $[SiW_{11}O_{39}]^{8-}$ (SiW_{11}), $(NH_4)_3PW_{12}O_{40}$ (NH_4-PW_{12}) and $(NH_4)_8Co_2W_{12}O_{42}$ (NH_4-Co_2W_{12}), for covalent combination with g-C_3N_4 (Zhao S. and Zhao X., 2019). All of the clusters significantly improved the charge separation of pristine PCN. Action spectra measurements revealed that the band excitation results in the generation of H_2O_2 in both g-C_3N_4 and g-C_3N_4-CoWO systems (Han X.-B. et al., 2015; Zhao S. et al., 2017; Zhao S. and Zhao X., 2019), indicating that the function of POM incorporation may be as the same as that of ion doping since POM clusters are all well dispersed in the PCN matrix. The inner-panel charge transfer and the charge transfer between the layers may be significantly promoted by the introduction of highly dispersed POM clusters.

3.1.3 Defect engineering

Recently, it was found that defects in semiconductors enhance photocatalytic activity if they are precisely controlled (Pei Z. et al., 2013; Xiong J. et al., 2018; Meng A. et al., 2020). Introduction of carbon vacancies (Li S. et al., 2016; Goclon J. and Winkler K., 2018) and introduction of nitrogen vacancies are usually defect engineering used in a g-C_3N_4 photocatalyst (Li X. et al., 2018b; Qu X. et al., 2018; Shi L. et al., 2018; Zhu Z. et al., 2018). These strategies can change the electronic configuration and reactant molecules to promote H_2O_2 production. For example, Li et al. synthesized g-C_3N_4 functionalized carbon vacancies (Cv-g-C_3N_4) through thermal annealing in an oxygen-deficient environment (Ar flow) (Li S. et al., 2016). This Cv-g-C_3N_4 was also functionalized with a large number of amino groups with the formation of carbon vacancies (Li S. et al., 2016). Under visible light irradiation (Kessler F.K. et al., 2017), the H_2O_2 yield of Cv-g-C_3N_4 was much higher than that of pure g-C_3N_4 (Li S. et al., 2016). The improved photocatalytic activity of Cv-g-C_3N_4 for H_2O_2 production can be ascribed to the promoted charge separation and alteration of the H_2O_2 production pathway from a stepwise $1e^-$ to $1e^-$ pathway to a $2e^-$ pathway.

Nitrogen vacancies in g-C_3N_4 can also boost the photocatalytic activity for H_2O_2 production (Zhu Z. et al., 2018). Li et al. (Li X. et al., 2018b) and Qu et al. (Qu X. et al., 2018) showed that nitrogen vacancies can be introduced in the matrix of g-C_3N_4 by dielectric barrier discharge (DBD) plasma treatment. Their results showed that H_2O_2 evolution can be improved by up to 10 times compared with that produced by pristine PCN (Li X. et al., 2018b). In another related study, Shi et al. created a holey defective C_3N_4 photocatalyst with nitrogen vacancies via a hydrazine photoreduction method. The transfer of charge carriers from the bulk to the surface was significantly improved, as confirmed by PL measurements (Shi L. et al., 2018). The introduced nitrogen vacancies narrowed the bandgap and the formation of defect states within the bandgap together with a notably suppressed electron-hole recombination. Therefore, the holey defective g-C_3N_4 photocatalyst showed much higher photocatalytic activity for visible light-driven H_2O_2 production than that of pristine g-C_3N_4.

In summary, the functionalization strategies of doping and defect engineering for improving the charge separation for PCN-based materials used for the $2e^-$ ORR process are similar to the functionalization strategies for other reactions such as HER, COR, and ORR. However, the hybridization of PCN-based materials, especially hybridization with electron-deficient semiconductors, provides a PCN-based photocatalyst with unique electronic properties for improving the charge separation. We believe that copolymerization strategies to introduce other electron-deficient groups with higher charge separation efficiency might enable the generation of π-conjugated and π-stacked donor–acceptor couples (Shiraishi Y. et al., 2019) in the PCN matrix, leading to a higher efficiency for photocatalytic H_2O_2 synthesis.

3.2 Improving light harvesting

Although pristine PCN can use visible light for a photocatalytic reaction, the large band gap (2.7 eV) results in insufficient visible light harvesting for further efficiency improvement (Ong W.-J. et al., 2016). Thus, improving the light absorbance of a g-C_3N_4-based photocatalyst and narrowing the band gap are two practical strategies for H_2O_2 production.

Copolymerization of PCN with other organic molecules/semiconductors, such as triazine, barbituric acid and aromatic diimides, not only improves the light absorbance of the photocatalyst but also narrows the bandgap. As mentioned in **Section 3.1.1.3**, Shiraishi and co-workers prepared a series of PCN samples hybridized with atomic diimides with a significantly narrowed band gap from 2.7 eV of pristine PCN to 2.4 eV of PCN/PDI (Shiraishi Y. et al., 2014a; Kofuji Y. et al., 2017; Kofuji Y. et al., 2016a). The light absorbance of PCN samples hybridized with aromatic diimides improved to about ~20 % at λ = 400 nm, indicating improved light absorption. Additionally, Ohno and co-workers co-polymerized melem with barbituric acid to expand the light absorption edge from 445 nm (2.76 eV) of pristine PCN to ~550 nm (2.18 eV) of PCNBA0.5 (**Fig. 11a**) (PCNBA is an abbreviation for polymetric carbon nitride doped by barbituric acid, 0.5 means calcination of 3 g melamine and 0.5 g barbituric acid) (Teng Z. et al., 2020). The absorbance of PCNBA0.2 at 420 nm was also increased by 200 % compared with that of pristine PCN (**Fig. 11b**) (Teng Z. et al., 2020).

Doping of alkaline metal ions can also expand the light absorption to a small extent (0.1 eV~0.3 eV) combined with significantly light improved absorbance (50 %). Alkaline metal doping and non-metal doping were also proved to be efficient strategies for improving light absorbance (Moon G.-h. et al., 2017; Kim S. et al., 2018; Zhang P. et al., 2020). Choi and co-workers found that the light absorption ability of CN samples was gradually promoted by increasing the amount of KPF_6, even though KPF_6 alone did not exhibit any visible-light absorption (Moon G.-h. et al., 2017) (**Fig. 11c**). A very recent work using K and S-co-doped PCN with functionalization of the –OH group (AKMT) also showed significant improvement in both light absorption and narrowing of the bandgap (Zhang P. et al., 2020). The light absorption edge expanded from ~450 nm of pristine PCN to ~520 nm of AKMT (Zhang P. et al., 2020) (**Fig. 11d**). With the addition of a sacrificial reagent, AKMT showed apparent quantum yields (AQYs) of 76 % and 40 % at 480 nm and 500 nm for H_2O_2 production, respectively. By comparison, pristine PCN exhibited negligible activities at the same wavelengths.

Defect engineering can also slightly improve the light absorption of photocatalysts, especially for semiconductor-based materials (Li S. et al., 2016) and Zhu et al. (Zhu Z. et al., 2018) reported that the UV-vis absorption spectra of

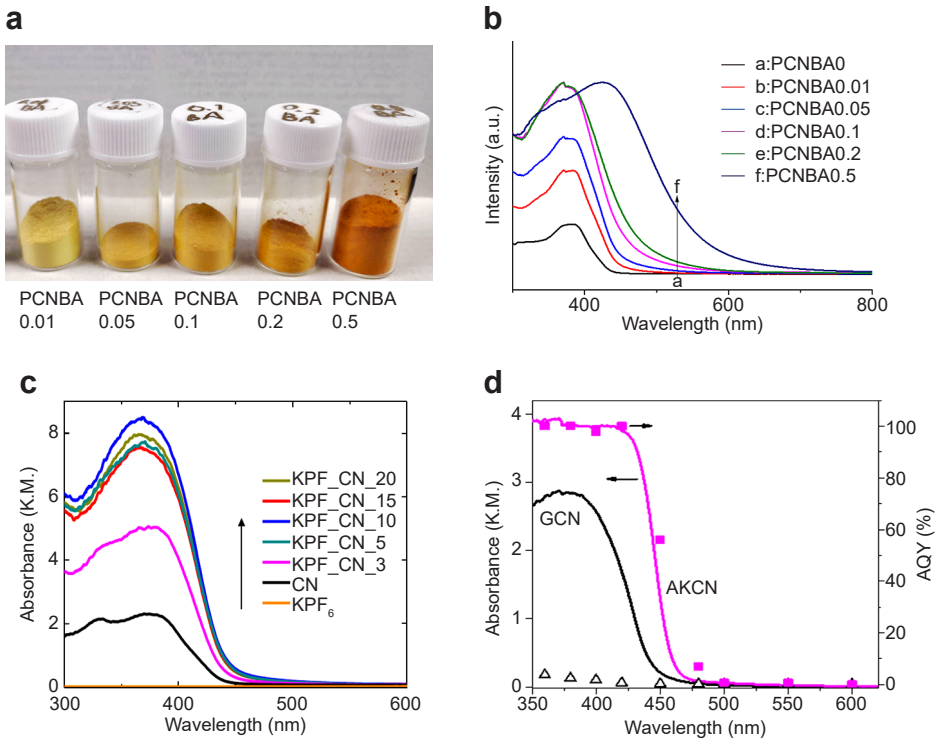

Fig. 11 Typical strategies for improving light harvesting. **(a)** Photographs show the corresponding powders of PCNBA samples. **(b)** UV-vis spectra of PCN and PCNBA samples: absorbance spectra. **(c)** Diffuse reflectance UV-vis spectra (DR-UVS) of modified CN samples prepared with various KPF_6 contents. **(d)** UV-vis spectra and apparent quantum yield (AQY) of H_2O_2 production as a function of irradiation wavelength with 10 % EtOH (v/v) under visible light irradiation ($\lambda \geq 420$ nm) and T = 25 °C. Reprinted with permission from Ref. (Teng Z. et al., 2020; Zhang P. 2019). Copyright: (2019) Springer Nature Ltd. and (2020) Elsevier.

g-C_3N_4 and carbon vacancy-functionalized g-C_3N_4 showed a red shift of absorption edges compared with that of pristine ones. Nitrogen vacancies also significantly improve light absorption (Li X. et al., 2018b; Qu X. et al., 2018; Shi L. et al., 2018). Ye and co-workers compared the optical properties of bulk PCN (BCN) and those of N-defected CN samples (DCN) (Shi L. et al., 2018). The absorption edges of the samples showed red shifts of ~40 nm compared with that of pristine g-C_3N_4 samples without thermal treatment (Shi L. et al., 2018). They also revealed that the electrons could be accommodated by forming defect states in BCN, which greatly promoted light harvesting (Shi L. et al., 2018). Compared with the copolymerization of an electron-deficient semiconductor and metal/non-metal doping, the influence of defect engineering is relatively small because defect states are usually located just below the CBM. In this case, the extent of narrowing of the bandgap by introducing defects is limited. Copolymerization of electron-deficient semiconductors seems to be the most promising functionalization strategy for both improving light absorbance and expanding the absorption edge.

3.3 Introduction of active sites for selective 2e⁻ ORR

Introduction of active sites with specific physicochemical properties can significantly improve both selectivity and activities (Bo Y. et al., 2020). To give a systematic review for this topic, three dominant strategies for introducing active sites for photocatalytic H_2O_2 production are presents as follows.

3.3.1 Increasing the surface area

PCN prepared by the thermal polymerization method is usually quite small (<15 $m^2 g^{-1}$) (Teng Z. et al., 2017). As previously mentioned, the conjugated heptazine ring in the PCN matrix can provide active sites for 2e⁻ ORR (Shiraishi Y. et al., 2014a). A plausible strategy for increasing the number of active sites for 2e⁻ ORR is to increase the surface area (Mohamed N.A. et al., 2019; Ou H. et al., 2017; Liao G. et al., 2019). However, there is still some controversy about whether the overall 2e⁻ ORR rate can be improved by increasing the specific surface area of PCN. Shiraishi and co-workers investigated the photocatalytic production of H_2O_2 with the existence of O_2 and Et-OH. A series of mesoporous g-C_3N_4 catalysts having different specific surface areas (SSA) were prepared by a hard template (silica nanoparticles with different diameters) method (**Fig. 12a**) (Shiraishi Y. et al., 2015). In these systems, photogenerated holes oxidize Et-OH and the conduction band electrons localized at the melem unit reduce O_2 to form H_2O_2. This g-C_3N_4 catalysts exhibit significant higher SSA of 56 and 160 $m^2 g^{-1}$ compared with that of pristine g-C_3N_4 (10 $m^2 g^{-1}$) and higher activity for H_2O_2 production (Shiraishi Y. et al., 2015). However, g-C_3N_4 with the largest SSA (228 $m^2 g^{-1}$) showed significantly decreased activity and selectivity for H_2O_2 formation (**Fig. 12b**) (Shiraishi Y. et al., 2015). Mesoporous g-C_3N_4 with the largest surface area inherently contains the largest number of primary amine moieties (Shiraishi Y. et al., 2015). The H_2O_2 selectivity was significantly suppressed since these defects can also serve as active sites for 4e⁻ reduction of O_2 (**Fig. 12c**) (Shiraishi Y. et al., 2015). These defects also further decomposed the formed H_2O_2, leading to significantly suppressed activity. Results of density function theory (DFT) calculations confirmed (i) a large distribution of lowest unoccupied molecular orbital (LUMO) electrons onto the primary amine moieties and (ii) a decrease in H_2O_2 selectivity with an increase in the amount of primary amine moieties, strongly suggesting that the primary amine moieties on the surfaces of mesopores behave as the active sites for four-electron reduction (**Fig. 12d–f**) (Shiraishi Y. et al., 2015). However, the specific types of those defects were not described in their reports. Specification of the types and fine structures of defects is important to further improvement by defect engineering strategies.

3.3.2 Copolymerization with electron-deficient semiconductors

Copolymerization with electron-deficient semiconductors such as PDI, BDI and MTI has also been proved to be one of the most efficient strategies for promoting the selectivity of a photocatalyst (Shiraishi Y. et al., 2014a; Kofuji Y. et al., 2017; Kofuji Y. et al., 2016a). Calculations based on the density functional theory (DFT) were investigated to clarify the influence of the PDI unit on the electronic structure of the g-C_3N_4 framework (Shiraishi Y. et al., 2014a). Time-dependent results showed that the main transitions are $S_0 \rightarrow S_1$ (highest occupied molecular orbitals, HOMO →LUMO and HOMO→LUMO+2). The iso-surfaces showed that electron distributions of the melem-PDI model (main transitions HOMO→LUMO+2) are located mainly at the melem units with partial distribution to the PDI units (Shiraishi Y. et al., 2014a). The high electron affinity of the PDI units in g-C_3N_4/PDI may significantly improve the polarization of the whole frameworks.

Being specific, the electrons on HOMO are concentrated at the N2 and N6 atom positions of the melem unit, and those on LUMO+2 are located at the C1 and N4 atoms (Shiraishi Y. et al., 2014a). The Raman spectra of g-C_3N_4/PDI and g-C_3N_4 confirmed that the side-on adsorption of O_2 was significantly promoted on g-C_3N_4/PDI, indicating a crucial role of copolymerization of electron-deficient semiconductors.

3.3.3 Doping/Heteroatom incorporation

Incorporation of metal species or no-metal species in the PCN matrix can both improve the charge separation and introduce active sites for specific reactions (Hu S.

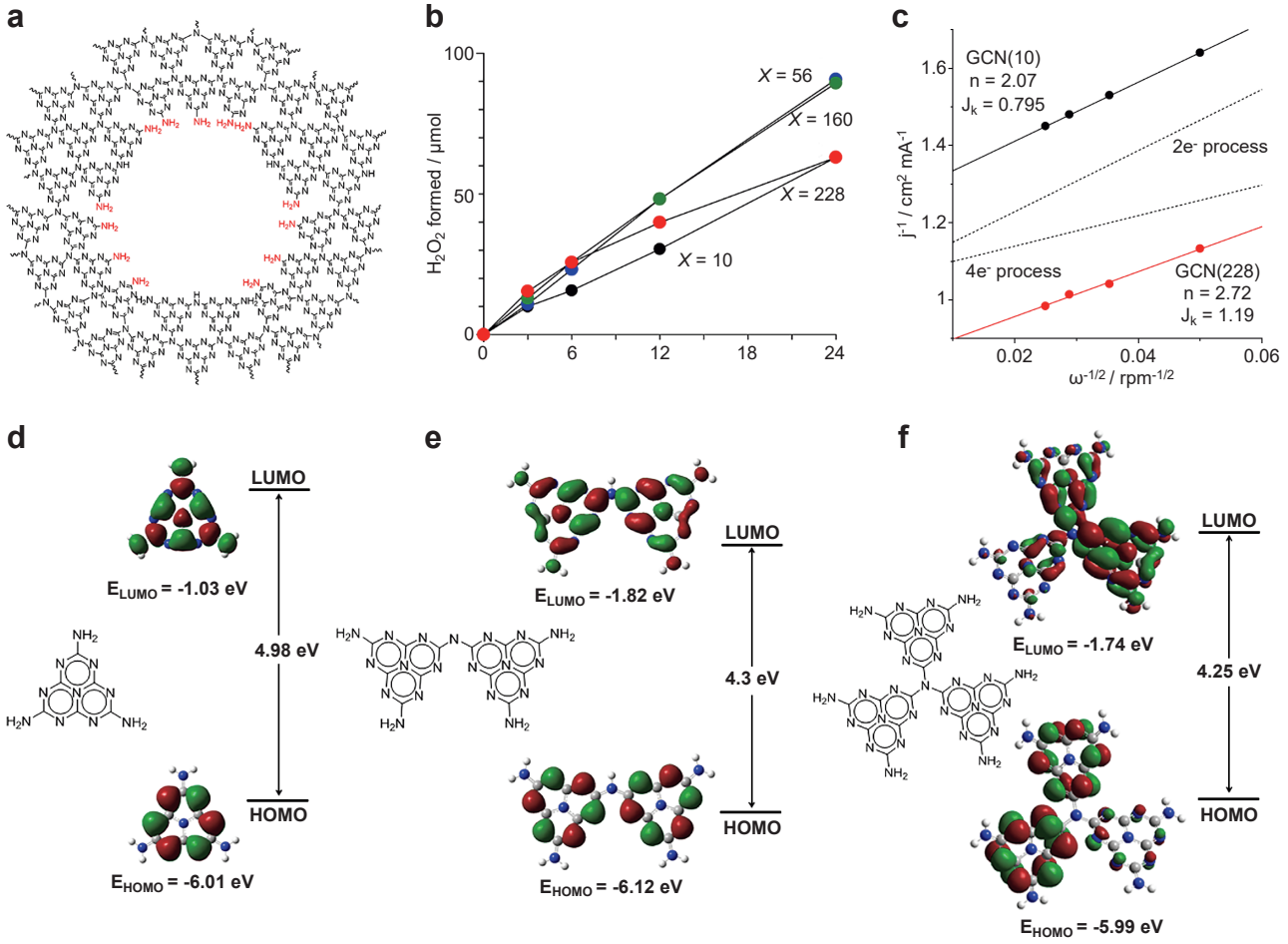

Fig. 12 Influence of surface defects on H_2O_2 production by using a PCN-based material. **(a)** Different N atoms of PCN. **(b)** Time-dependent change in the amounts of H_2O_2 during photoreaction on the respective GCN(x) catalysts. **(c)** Electron transfer numbers during the photocatalytic H_2O_2 production. Interfacial plots of the main orbitals for **(d)** single, **(e)** double, and **(f)** triple melem-conjugated models, calculated by the function of B3LYP at the 6-31G **(d)** level. Reprinted with permission from Ref. (Shiraishi Y. et al., 2015). Copyright: (2015) American Chemical Society.

et al., 2018; Zhang Z. et al., 2022). By the template-assisted method, Hu and co-workers fabricated hollow copper-doped g-C_3N_4 microspheres. The g-C_3N_4 with copper incorporation showed a much higher H_2O_2 production ability (~4.8 mmol·L^{-1}) than that of pristine g-C_3N_4 (0.45 mmol·L^{-1}). DFT simulations showed that the Cu(I)-N sites work as reactive sites to activate molecular O_2 (Hu S. et al., 2018). The OCN proposed by Zhu and co-workers was proven to show a high selectivity for 2e$^-$ ORR for photocatalytic H_2O_2 production, which is attributed to the functionalized C-O-C groups on OCNs (Wei Z. et al., 2018). Choi and co-workers revealed by DFT calculations that the K incorporation could result in improved adsorption for O_2 molecules (Zhang P. et al., 2019) (**Fig. 13a, b**). They also investigated whether electrons on S-doped g-C_3N_4 can be donated to the antibonding π* orbital of adsorbed *O_2 (with –0.40 |e|) for forming efficient ORR sites, as well as AQ doping as cocatalysts (**Fig. 13c**). The strong electron pushing effect between carbon and oxygen facilitates subsequent protonation in ORR kinetics (Chu C. et al., 2020). Both the activity and selectivity of ORR can be changed by manipulating the properties of metallic sites (Kulkarni A. et al., 2018). As elaborated in several electrochemical catalysts, the end-on O_2 adsorption usually lead to highly selective 2e$^-$ ORR. It is difficult to prevent the splitting of O-O bond breaking on surface of metal particles since end-on O_2 molecular adsorption and side-on O_2 molecular adsorption occur on metal particles (Choi C.H. et al., 2014; Chu C. et al., 2019). Benefiting from the desirable features of a single atom catalyst (SAC) (Sun H. et al., 2021), the adsorption of O_2 molecules on atomically isolated sites is often end-on type, which could reduce the possibility of O-O bond splitting (Kulkarni A. et al., 2018; Wang A. et al., 2018). For example, SACs with Pt^{2+} (Shen R. et al., 2019) and Co-N_4 (Gao J. et al., 2020; Jung E. et al., 2020) centers could electrochemically reduce O_2 to H_2O_2 via a 2e$^-$ ORR pathway with ultrahigh selectivity (>96 %). However, it is difficult for Pt^{2+} and Co-N_4 sites to be coupled in the photocatalytic system due to their high charge recombination characteristics, which originate from the intermediate band formed by the half-filled d electrons (Teng Z. et al., 2021a). Very recently, Ohno and co-workers

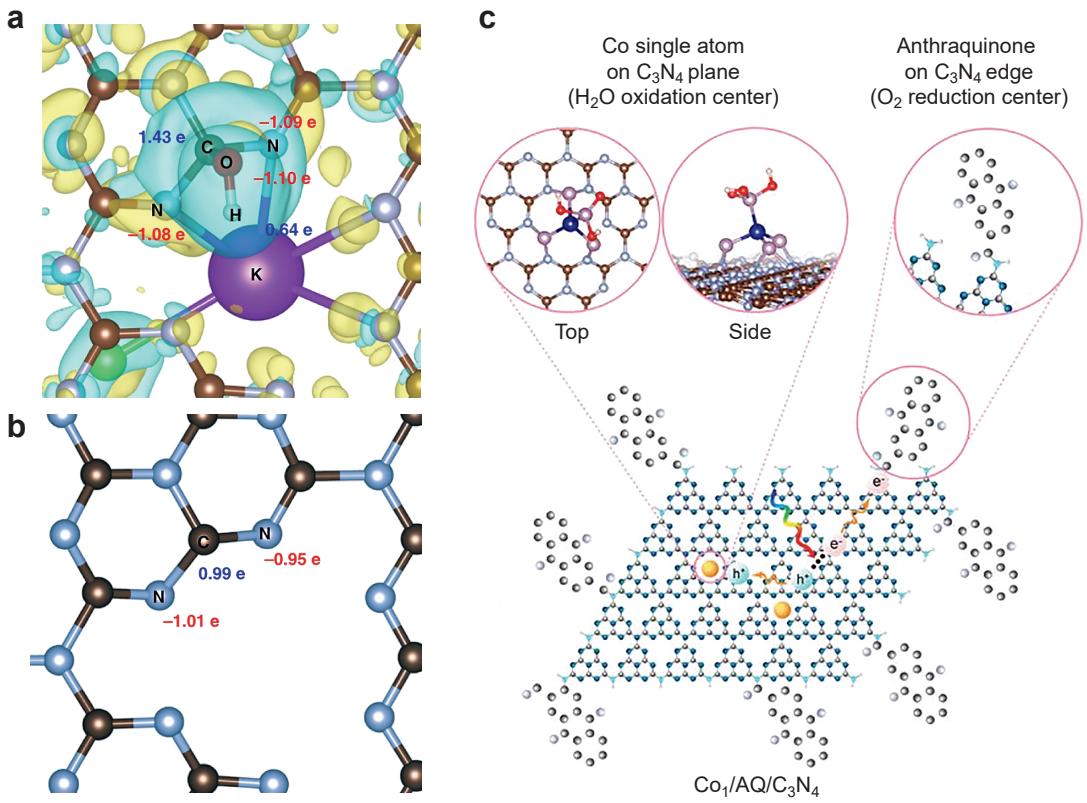

Fig. 13 Typical strategies for introducing active sites for efficient 2e⁻ ORR. **(a)** An enlarged top view of KCl-OH-GCN, and **(b)** an enlarged top view of pristine GCN. The yellow and blue colors represent electron accumulation and depletion at an isosurface value of 0.002 Å e^{-3}. The brown, gray, and violet colors represent carbon, nitrogen, and potassuim, respectively. **(c)** Spatial separation of Co single atom (as an oxidation center) and AQ (as a reduction center) cocatalysts by anchoring them in the center (i.e., pyridinic N) and on the edge (i.e., primary/secondary amine N) of 2D ultrathin C_3N_4. Reprinted with permission from Ref. (Zhang P. et al., 2019; Chu C. et al., 2020). Copyright: (2019) Springer Nature Ltd. and (2020) The Authors (Chu C. et al.), published by National Academy of Science.

developed an Sb single atom photocatalyst (Sb-SAPC) for non-sacrificial photocatalytic H_2O_2 synthesis in a water and oxygen mixture under visible light irradiation (Teng Z. et al., 2021a). The Sb-SAPC was prepared by a wet chemical method using $NaSbF_6$ and melamine as precursors. As shown in the image acquired from high-angle annular dark field scanning TEM (HAADF-STEM) measurement, the bright spots with high density are uniformly dispersed in the entire carbon nitride matrix (**Fig. 14a**). Electron energy loss spectroscopy (EELS) (**Fig. 14b**) measurement revealed bright spots corresponding to Sb atoms, in which the oxidation state of Sb is regulated to +3 with a $4d^{10}5s^2$ electron configuration (**Fig. 14c, d**). The results of experimental and theoretical investigations indicated that the adsorption of O_2 on isolated Sb atomic sites is end-on type, which promotes the formation of Sb-μ-peroxide (Sb-OOH), leading to an efficient 2e⁻ ORR pathway for H_2O_2 production (**Fig. 14e**). The 2e⁻ ORR efficiency of Sb species improved by almost one magnitude in the presence of 2-propanol (**Fig. 14f**). The apparent charge recombination of Sb-SAPC was significantly suppressed by introducing Sb species into the PCN matrix (**Fig. 14g, h**). With highly concentrated holes, this catalyst also achieved non-sacrificial H_2O_2 production using water as an electronic donor.

3.3.4 Cocatalyst loading

Cocatalyst loading is a traditional strategy for introducing active sites for specific reactions (Nosaka Y. and Nosaka A, 2016). For instance, pristine PCN shows quite low efficiency in photocatalytic hydrogen production, and loading of platinum species on PCN usually significantly improves the HER performance (Wang Q. and Domen K., 2020). The reason for loading a cocatalyst to boost the photocatalytic reactions is usually the decreased overpotential of the reactions on the co-catalyst surface compared with that on pristine photocatalysts (Hirakawa H. et al., 2016; Tsukamoto D. et al., 2012; Peng Y. et al., 2017). AQ species can enhance the selectivity of O_2 reduction to H_2O_2 based on the mechanism of the current industrial H_2O_2 production process (Kim H.-i. et al., 2018; Chu C. et al., 2020). Kim and co-workers prepared several AQ-modified PCN samples with significantly improved selectivity for 2e⁻ ORR (Chu C. et al., 2020). Loading an AQ cocatalyst onto ultrathin g-C_3N_4 significantly improved the selectivity of H_2O_2 production, combined with a 1.9-fold enhancement of the amount of H_2O_2 production (Chu C. et al., 2020). Several works in which Au nanoparticles were loaded onto the C_3N_4 matrix all showed significantly improved 2e⁻ ORR efficiency (Chang X. et al., 2018; Zuo G. et al., 2019). This

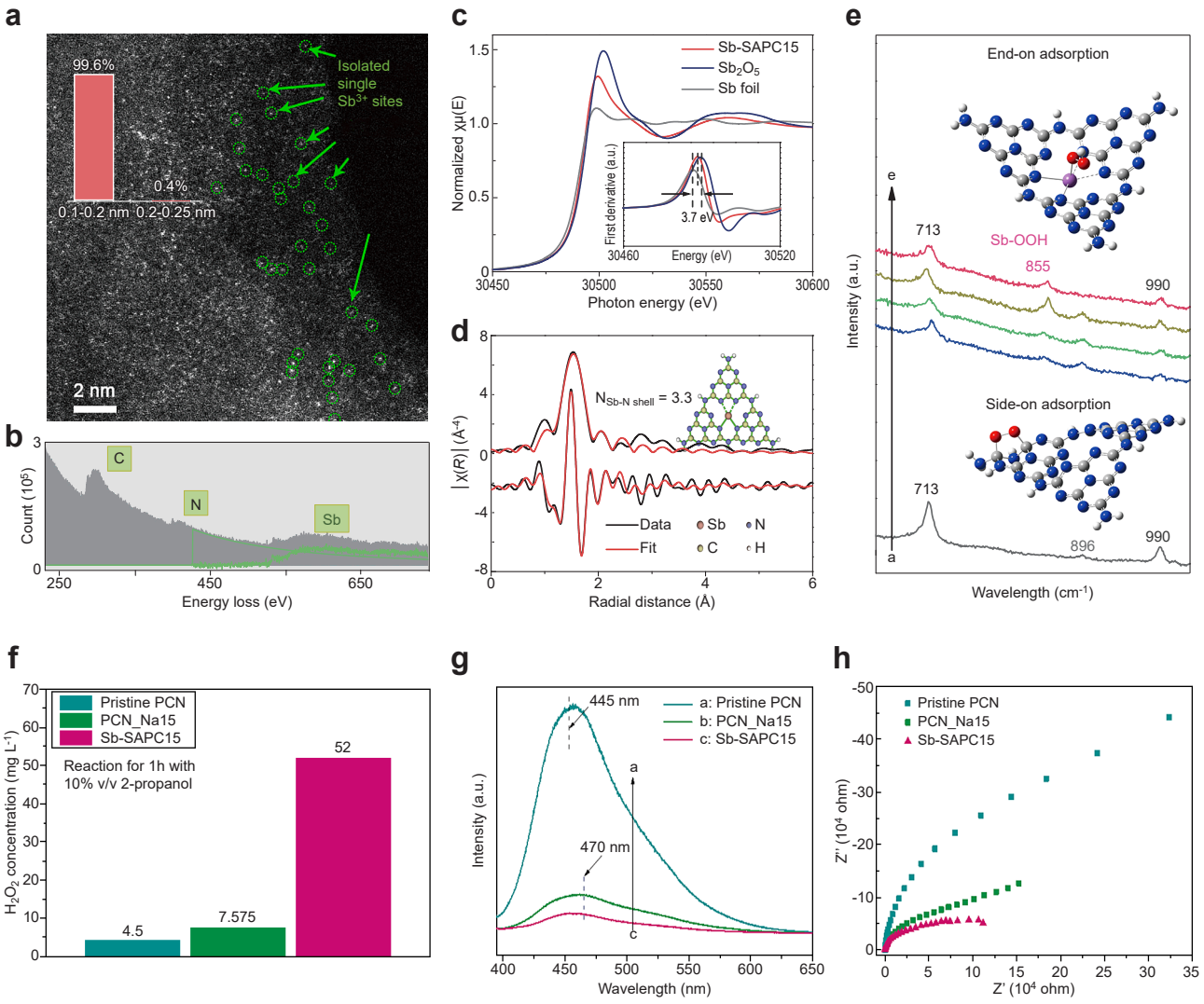

Fig. 14 Single atomic sites for efficient ORR. **(a)** High-magnification HAADF-STEM image of Sb-SAPC15. The insert shows size distribution of the bright spots. **(b)** Electron energy-loss spectroscopy (EELS) spectrum of Sb-SAPC15. **(c)** Sb-K edge X-ray absorption near edge structure (XANES) of Sb foil, Sb_2O_5 and Sb-SAPC15. **(d)** Fitting of the extended X-ray absorption fine structure (EXAFS) data for Sb-SAPC15 based on the model obtained from DFT optimization. Inserted figures: optimized molecular models based on DFT for EXAFS fitting. **(e)** Experimental Raman spectra recorded during the photoreaction in a 2-propanol aqueous solution with saturated oxygen. Spectra a, b, c and d: PCN, Sb-SAPC1, Sb-SAPC5 and Sb-SAPC15 in 10 % (v/v) 2-propanol aqueous solutions. Spectrum e: Sb-SAPC15 in pure water. **(f)** Comparison of H_2O_2 production in 10 % (v/v) 2-propanol aqueous solutions catalyzed by pristine PCN, PCN_Na15 and Sb-SAPC15. **(g)** Photoluminescence spectra of PCN, PCN_Na15 and Sb-SAPC15 at an excitation wavelength of 380 nm **(h)** Electrochemical impedance spectroscopy (EIS) spectra (Nyquist plots) of pristine PCN and Sb-SAPC15 in the frequency range from 100 kHz to 0.01 Hz at 0.6 V (vs. Ag/AgCl) under visible light irradiation. Reprinted with permission from Ref. (Teng Z. et al., 2021b). Copyright: (2021) Springer Nature Ltd.

phenomenon may be attributed to the cocatalytic effects of the Au surface on the photocatalytic 2e⁻ ORR, which has already been proved by investigating other photocatalysts and photocathodes (Hirakawa H. et al., 2016).

In summary, there are two fundamental strategies for introducing active sites for the improvement of 2e⁻ ORR of a PCN-based photocatalyst. One is to manipulate the electronic configurations of the functionalized PCN catalyst so that the selectivity and activity of the π-conjugated heptazine ring for boosting H_2O_2 production can be significantly enhanced. Similar strategies have also been used in some other carbon-based materials for promoting selective H_2O_2 production. On the contrary, the nature of melem sites is side-on adsorption of oxygen (Shiraishi Y. et al., 2015), which might result in unexpected splitting of O-O bonds, thus leading to the possible 4e⁻ ORR process and a limited selectivity for 2e⁻ ORR (Siahrostami S. et al., 2013; Verdaguer-Casadevall A. et al., 2014). The other strategy is to introduce active sites beyond the π-conjugated heptazine ring for selective 2e⁻ ORR. Up to now, only a few cocatalysts have been developed for selective ORR (**Section 3.3.4**). Further development of 2e⁻ ORR sites beyond the π-conjugated heptazine rings may overcome the disadvantage of side-on O_2 adsorption and shed light on further improvement for H_2O_2 production.

4. Other factors for boosting photocatalytic efficiency for H_2O_2 production

4.1 Adding electron donors or not

Sacrificial reagents are commonly used to consume the photogenerated electrons or holes so that half of the reaction can be significantly boosted (Schneider J. and Bahnemann D.W., 2013). In the case of g-C_3N_4-based photocatalysts, most researchers used electron donors so that reduction reactions could be maximized in a certain photocatalytic system since an electron donor prevents the photogenerated electrons from recombining with holes (Wang Y. et al., 2019; Wang M. et al., 2017). g-C_3N_4 has shown promising prospects for catalyzing several photochemical reduction reactions with the existence of electron donors. The reason may be as follows: the CBM of pristine PCN (–1.3 V) is quite negative, thus resulting in significantly larger redox potentials of hydrogen evolution reaction (HER), nitrogen reduction reaction (NRR), carbon dioxide reduction reaction (CRR) and 2e⁻ ORR (0.695 V vs. SHE) (Wang Y. et al., 2019). Combined with the merits of the side-on O_2 adsorption on melem units (forming 1-4 endoperoxide species) as acceptable 2e⁻ reduction sites, PCN satisfied the thermodynamic potential for 2e⁻ ORR with the existence of alcohol. However, a green and sustainable process for photocatalytic H_2O_2 synthesis requires the use of earth-abundant water as an electron donor, i.e., water oxidation reaction instead of alcohol oxidation should occur for hole consumption.

There have been several studies in which mechanisms for photoreduction reactions were systematically investigated by using g-C_3N_4 (Wang Y. et al., 2019). Since the functions of electron donors were clarified in those works, we will focus on the crucial properties and functionalization strategies for achieving H_2O_2 production with water and oxygen (**Fig. 15a**). Typically, water oxidation via a 4e⁻ pathway is usually recognized as an oxygen evolution reaction (OER) that is usually needed to overcome the large overpotential. VBMs of photocatalysts for OER usually have quite positive potentials ($VBM_{TiO2\text{-}rutile}$ ~2.9 V vs. SHE, VBM_{BiVO4} ~2.53 V) (Fan W. et al., 2020; Hirakawa H. et al., 2016). As shown in **Fig. 15b**, pristine PCN is unable to generate H_2O_2 in the presence of water and O_2 because the valence band maximum (VBM) lies at approximately 1.4 V, which shows an insufficient thermodynamic driving force for OER (ca. 0.8 V versus RHE, pH 7) (Shiraishi Y. et al., 2014a). To overcome this obstacle, band engineering and the use of a cocatalyst are two effective strategies.

The bandgap position of PCN can be easily manipulated

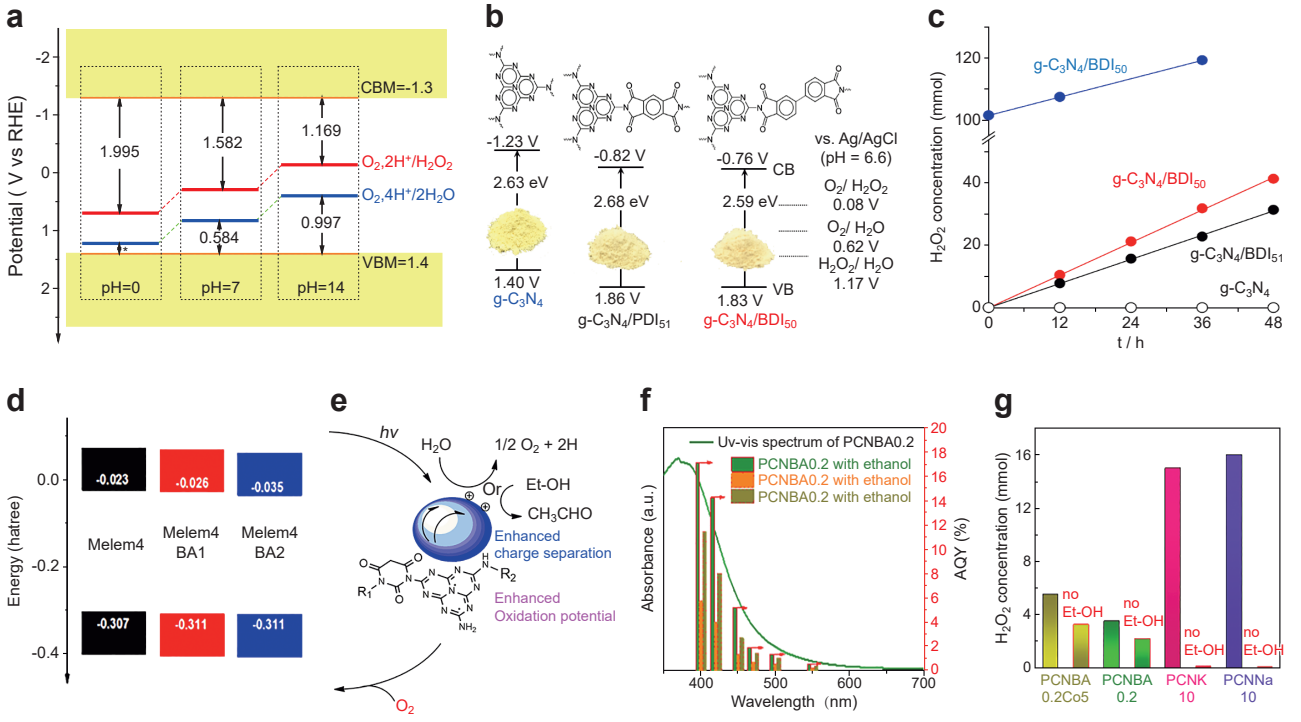

Fig. 15 Typical strategies for preparation of a g-C_3N_4-based catalyst for photocatalytic H_2O_2 production with water and O_2. **(a)** Real hydrogen electrode potentials of 2e⁻ ORR and 4e⁻ WOR compared with the band diagram of PCN. **(b)** Electronic band structures of pristine PCN and g-C_3N_4/BDI_x. **(c)** Changes in the amounts of H_2O_2 formed during photoreaction with respective catalysts. For the reaction in **(c)**, 100 mg of catalyst was used. The irradiance at 420–500 nm is 27.3 W m^{-2}. Blue points show the results of photoreaction with water containing ca. 100 μmol of H_2O_2. **(d)** Calculated HOMO and LUMO of Melem_4 model (representing PCN), Melem_4BA1 (representing PCNBA with a low motif concentration) and Melem_4BA2 (representing PCNBA with a high motif concentration). **(e)** Schematic diagram of $PCNBA_xCo_x$ for accelerating water oxidation. **(f)** Absorption spectrum of PCNBA0.2 and action spectra for H_2O_2 formation on the respective catalysts. **(g)** Time course of O_2 evolution measured under Ar pressure of 0.6-kPa and 300-W xenon lamp irradiation with 0.5 g L^{-1} of the catalyst, 1 g L^{-1} La_2O_3, and 20 mM $AgNO_3$ in 100 mL of water. Reprinted with permission from Ref. (Kofuji Y., et al., 2016b; Teng Z. et al., 2020). Copyright: (2016) American Chemical Society and (2020) Elsevier.

by functionalization. Shiraishi and co-workers successfully manipulate the band positions of a PCN-based photocatalyst by copolymerized melamine with electron-deficient aromatic diimide (Shiraishi Y. et al., 2014a; Shiraishi Y. et al., 2014b; Kofuji Y. et al., 2016a; Kofuji Y. et al., 2017; Kofuji Y. et al., 2016b). The valence band of the as-prepared co-polymerized PCN is about 1.8~2.4 V (vs. NHE). Taking g-C_3N_4/PDI as an example, the activity results revealed a significant role of band engineering. Pristine g-C_3N_4 (VBM = 1.40 V vs. NHE) barely produces H_2O_2, and g-C_3N_4/BDI51 (VBM = 1.86 V vs. NHE) produces 31 μmol of H_2O_2 after photocatalytic reaction for 48 h (Kofuji Y. et al., 2016b) (**Fig. 15c**). g-C_3N_4/BDI50 (VBM = 1.83 V vs. NHE) shows a higher performance (41 μmol) (Kofuji Y. et al., 2016b). With the addition of electron acceptors, O_2 can be detected by GC, which further confirmed that water oxidation to generate oxygen consumed the generated holes during the photocatalytic reactions (Kofuji Y. et al., 2016b). Introduction of boron nitride (BN) can further improve the activity of the g-C_3N_4/PDI-rGO photocatalyst because of the enhanced charge separation efficiency (Kofuji Y. et al., 2018). Following those works, Ohno and co-workers further revealed by analysis of the density of states that the copolymerization of electron-deficient units results in the introduction of O 2p states (Teng Z. et al., 2020). The introduced O 2p states compose the valence band with the states of N 2p and C 2p, resulting in a more positive potential than that of pristine PCN for which the VB is only composed of the states of N 2p and C 2p (**Fig. 15d**) (Teng Z. et al., 2020). Thus, the OER activity is significantly promoted (**Fig. 15e**). Additionally, preparation of POM-incorporated PCN samples with ideal electronic configurations and band positions also played similar roles (shifting the VBM to a more oxidative potential) for boosting the OER, which successfully achieved the H_2O_2 production via ORR and WOR (Zhao S. et al., 2018b; Zhao S. et al., 2017; Zhao S. and Zhao X., 2019). Another strategy for improving the OER activity of PCN is loading a cocatalyst for OERs. Ohno and co-workers loaded $Na_2CoP_2O_7$ on the band-engineered PCNBA0.2 by a simple ball milling method (**Fig. 15e**) (Teng Z. et al., 2020). The time-dependent H_2O_2 production and action spectra confirmed the cocatalytic effects of $Na_2CoP_2O_7$ (Teng Z. et al., 2020). The action spectra showed that its bandgap excitation produces H_2O_2 (Teng Z. et al., 2020). The apparent quantum yield (AQY) of PCNBA with loading of 5 % $Na_2CoP_2O_7$ (PCNBA0.2Co5 %) at 420 nm (8.0 %) was two-times higher than that of PCNBA0.2 (4.0 %) (**Fig. 15f**) (Teng Z. et al., 2020). Additionally, no H_2O_2 was produced at the light-irradiation wavelengths between 550 nm and 650 nm, indicating that $Na_2CoP_2O_7$ works as a cocatalyst and does not work as a photocatalyst for production of H_2O_2 (Teng Z. et al., 2020). More recently, Chu and co-workers prepared single-atom dispersed Co as a co-catalyst for OER (Chu C. et al., 2020). X-ray absorption fine-structure spectroscopy (FT-EXAFS) showed that the oxidation state of the Co single atoms coordinated by P atoms is close to +2 (Chu C. et al., 2020). The OER activity of g-C_3N_4 was significantly increased (8.4-fold) by the introduction of Co single atomic sites (**Fig. 15g**). The chemical states of P-coordinated Co atoms are close to +2, indicating that the unique electronic configuration of Co(II)-P may provide active sites for OER during solar H_2O_2 synthesis (Chu C. et al., 2020). It is notable that the VBM of this single-Co dispersed PCN (~1.4 V vs. SHE) (Chu C. et al., 2020), quite close to that of PCN, is significantly more positive than that of metal oxides (>2.3 V vs. SHE). Thus, the Co(II)-P single atomic sites may significantly boost the kinetic process of water oxidation. Very recently, the Sb-SAPC proposed by Ohno and co-workers also showed good activity based on non-sacrificial photocatalytic H_2O_2 activities. Based on the results detailed characterizations and analyses, the following reaction mechanism (**Fig. 16**) of Sb-SAPC for photocatalytic H_2O_2 production is proposed. Firstly, efficient charge separation occurs on Sb-SAPC under visible light irradiation, resulting in the generation of photoexcited electrons and holes for ORR and WOR, respectively. Then water molecules are oxidized to evolve O_2 by photogenerated holes localized at the N atoms near the single Sb atoms. Simultaneously, O_2 dissolved in water and that generated from the WOR both participate in the ORR process to produce H_2O_2. It is notable that the efficient charge separation, ideal single atomic sites for end-on type O_2 adsorption and close spatial distribution of active sites boost both the $2e^-$ ORR and $4e^-$ WOR for efficient H_2O_2 production.

In summary, accelerating the photocatalytic oxygen evolution reaction by using a PCN-based photocatalyst is the most crucial challenge for achieving photocatalytic H_2O_2 production with water and O_2. Band engineering and loading cocatalyst for OER may respectively improve the oxidation potential and promote the kinetics for $4e^-$ OER.

4.2 pH value

It is difficult for the light-driven $2e^-$ WOR pathway to be achieved because of the uphill thermodynamics (1.76 V vs. NHE), i.e., the as-synthesized H_2O_2 will decompose at this highly oxidative potential because H_2O_2 is an excellent hole scavenger (Fuku K. and Sayama K., 2016). Therefore, we will focus on the $2e^-$ ORR pathway. Substantial efforts have been devoted to the $2e^-$ ORR concept with the aim of achieving high-yield production of H_2O_2 in basic, neutral, and acidic media (Gao J. and Liu B., 2020; Kim H.W. et al., 2018; Lu Z. et al., 2018; Iglesias D. et al., 2018). The acid dissociation constant of H_2O_2 ($H_2O_2 \leftrightarrow H^+ + HO_2^-$, $K_a = \frac{[H^+][HO_2^-]}{[H_2O_2]}$, $pK_a = 11.7$) suggests that the main form of H_2O_2 would be HO_2^- in an alkaline

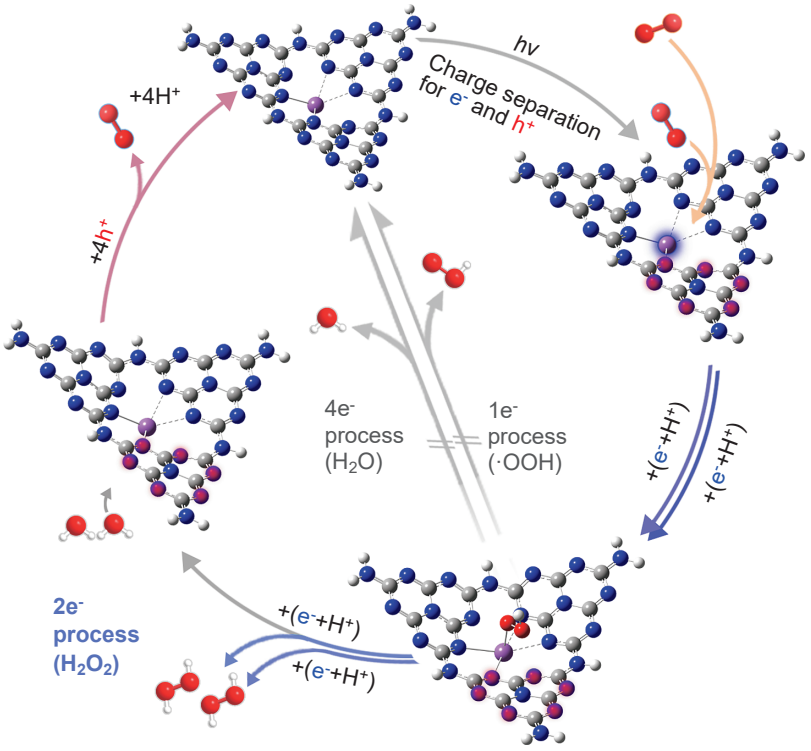

Fig. 16 Mechanism of photocatalytic H_2O_2 production. (White, gray, blue, red and magenta spheres indicate hydrogen, carbon, nitrogen, oxygen and Sb atoms, respectively.) After shining visible light, the photogenerated electrons are localized at the Sb sites (with a blue glow), and the photogenerated holes are localized at the N atoms at the melem units (with a red glow). Subsequently, the dissolved O_2 molecules are adsorbed (orange arrows) onto the Sb sites and then become reduced (blue arrows) via a $2e^-$ transfer pathway through the formation of an electron μ-peroxide as the intermediate. Simultaneously, water molecules are oxidized (pink arrows) to generate O_2 by the highly concentrated holes on the melem units. Reprinted with permission from Ref. (Teng Z. et al., 2021b). Copyright: (2021) Springer Nature Ltd.

water solution (pH >11.7). Alkaline H_2O_2 is widely used in the pulp bleaching industry. However, the production of H_2O_2 in basic media has the following two limitations: (1) H_2O_2 is less stable and can self-decompose in an alkaline condition (especially at pH >9), and it therefore needs to be consumed in a short time (Gao J. and Liu B., 2020; Qiang Z. et al., 2002) and (2) H_2O_2 is more widely used in natural or acidic media with stronger oxidation ability than in an alkaline solution. For instance, Fenton's reagent, which is widely used in effluent treatment and organic synthesis, has a favorable pH range of 2.5–3.5 (Gao J. and Liu B., 2020; Kuo W.G. et al., 1992). Therefore, improving H_2O_2 production in acidic or neutral media by photocatalysts has attracted much attention for industrial applications. Over the past few years, although various g-C_3N_4 catalysts have been developed for H_2O_2 production via the $2e^-$ ORR process (Shiraishi Y. et al., 2014b), there have been very few works in which the optimized pH conditions were investigated.

Kim and co-workers found that photocatalytic activity for H_2O_2 production was higher at lower pH values (**Fig. 17a**) with the existence of an electron donor. This is probably due to proton conduction within the CN framework and is much more facilitated in KPF_CN. The proton conduction of KPF_CN was greatly enhanced when PF_6^- anions was introduced into the structure of the g-C_3N_4 framework (Kim S. et al., 2018). The higher charge carrier density in KPF_CN might be favorable for facilitating proton conduction. The higher proton conductivity within the KPF_CN framework promotes the production of H_2O_2, particularly when the reaction between O_2 and protons occurs within the interlayer space (Kim S. et al., 2018). Ohno and co-workers also investigated the optimal pH conditions by measuring the amount of H_2O_2 produced by the photocatalytic reaction using PCNBA0.2 (**Fig. 17b**) (Teng Z. et al., 2020). When ethanol was introduced into the system, the amount of produced H_2O_2 remained almost constant when the pH value was increased from 1 to 9 and then decreased drastically (Teng Z. et al., 2020). When the pH value was lower than 7, the concentration of protons had almost no effect on the pH value (Teng Z. et al., 2020). This phenomenon revealed that protonation plays a less essential role in the PCNBA system, indicating that incorporation of BA units further improved the proton conductivity compared with that of KPF_CN. They also found that the lowest $[H^+]$ is 10^{-9} mol L^{-1} for O_2 reduction to H_2O_2 production. When no sacrificial agent was added to the system, the amount of H_2O_2 rapidly increased before the pH value reached 7 and then gradually decreased, indicating that a low concentration of OH^- also restricts the generation

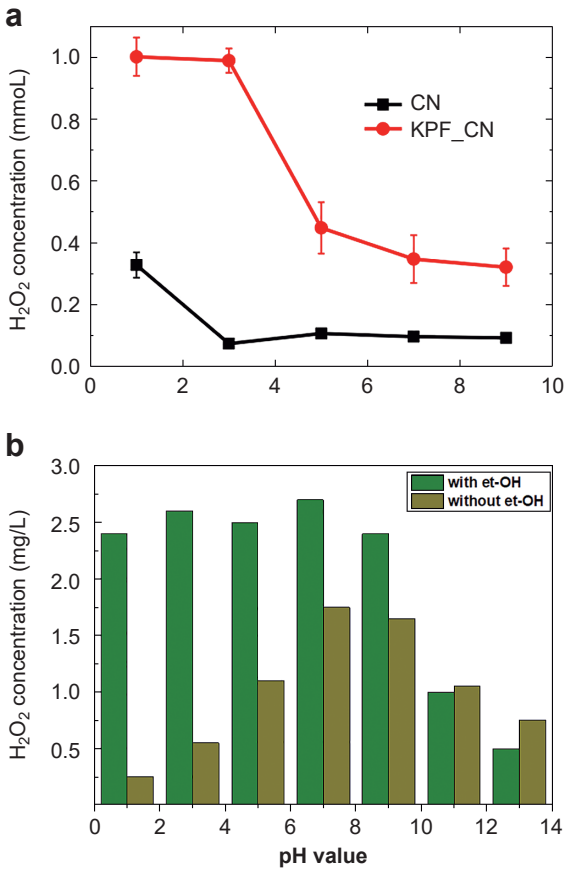

Fig. 17 Influence of pH values during H_2O_2 production by using a PCN-based photocatalyst. **(a)** H_2O_2 production in an irradiated suspension of bare CN and KPF_CN_15 at different pH values. **(b)** Optimization of the pH condition for H_2O_2 production when PCNBA0.2 was used as a photocatalyst. Reprinted with permission from (Kim S. et al., 2018) and (Teng Z. et al., 2020). Copyright: (2018, 2020) Elsevier.

of O_2 from water (Wang Q. and Domen K., 2020). Therefore, the optimal pH condition for H_2O_2 production from O_2 and water using PCNBA is 7-9. The production of H_2O_2 significantly decreased in both of the works when pH was larger than 9, being consistent with the fact that H_2O_2 self-decomposes in alkaline conditions. Although there have been only few works in which the influence of pH on the amount of H_2O_2 generated was investigated, it was shown that the pH value did play an essential role during the photosynthesis process. Additionally, the pH value of the interfaces between materials and reaction solution might be even more important compared with the pH value of the whole solution. The rational design of Helmholtz layer by the manipulation of the surface properties are extremely important for improving the H_2O_2 production (Zeng X. et al., 2020). We believe that systematic investigations of the effects of pH on the amount of H_2O_2, surface properties and electronic configurations should be carried out to reveal the mechanisms of ORR and WOR during the photosynthesis of H_2O_2.

5. Summary and perspectives

Photocatalytic H_2O_2 production by using a PCN-based material has shown a promising prospective in environmental and energy-related realms. We have summarized the principles for photocatalytic H_2O_2 production, especially for the photocatalytic H_2O_2 production using g-C_3N_4. Advantages and disadvantages for H_2O_2 production and the most favorable properties of PCN for photocatalytic H_2O_2 production were briefly summarized. Based on the intrinsic properties of pristine g-C_3N_4, the most urgent issue for overcoming the drawbacks was focused on. Notably, current PCN-based photocatalysts still suffer from relatively low H_2O_2 yield. Due to the low activity, g-C_3N_4-based photocatalysts are far from the requirements for industrial applications. Improving the charge separation, promoting the light absorption and introducing active sites for $2e^-$ ORR to suppress the side reaction are three attractive strategies for boosting the activities. Following discussion of these strategies, the most representative functionalization method was summarized on the basis of the most desired properties for improving the photocatalytic activities for H_2O_2 production. Other factors for improving H_2O_2 production such as addition of electron donors and pH value of the solution were also discussed.

There are several outlooks and suggestions for further improvement of photocatalysts. First of all, further improvement in the charge separation of the PCN is necessary. New species of elements or organic semiconductors for incorporation are highly recommended. Secondly, the absorption edge of the functionalized PCN can hardly be extended to >550 nm with a reasonable AQY for H_2O_2 production (Teng Z. et al., 2020). Further narrowing of band gap is therefore still of great importance. It is notable that the narrowing of the bandgap could reduce the thermodynamic driving force, leading to weakened capability for reduction reactions and oxidation reactions. Thus, reducing the overpotential for $2e^-$ ORR and oxidation reactions on the PCN surface is of great importance. Exploring new reaction sites with higher performance beyond the heptazine rings in the PCN matrix for $2e^-$ ORR efficiency is also of great importance for further improvement of photocatalytic activity and selectivity for H_2O_2 production. Recently, single-atom catalysts (SACs) have shown excellent selectivity for H_2O_2 production with Pt^{2+} (Shen R. et al., 2019; Gao J. et al., 2020; Jung E. et al., 2020) via a $2e^-$ ORR pathway. In the case of PCN, anchoring single-atom catalysts that have large amounts of nitrogen atoms with lone electron pairs is easy to perform. However, Pt^{2+} and Co-N_4 sites can hardly be utilized for photocatalytic systems due to poor charge separation, which origin form the half-filled d electrons of Pt^{2+} and Co-N_4 may result in a high bulk-recombination rate of PCN. The preparation of photocatalysts having atomically dispersed atoms with a d^0 or d^{10} electronic configuration usually introduce intermediate bands with

energetic levels that are slightly more negative than that of CBM, which can promote electron mobility, thus leading to a boosted performance (Inoue Y., 2009). It should be mentioned that measurement of H_2O_2 production was carried out in most studies with the addition of an organic sacrificial electron donor to consume the photogenerated holes and inhibit the recombination of photogenerated carries, which is energy-consuming and cost-inefficient. Despite of band engineering and cocatalyst loading, the construction of an all-solid-state Z-scheme photocatalytic system is another recommended strategy for achieving non-sacrificial H_2O_2 production with water and oxygen (Xu Q. et al., 2018). Additionally, it is necessary to develop approaches other than optimization of pH conditions to prevent decomposition of the generated H_2O_2. The stability of organic semiconductors during photocatalytic H_2O_2 production should also be investigated (Liu L. et al., 2021). Last not but least, attention should be given to precise determination of the amount of H_2O_2 generated because the species in the solution can influence the accuracy for determination (Wei Y. et al., 2021).

To optimize the design of functionalized PCN with maximized photocatalytic H_2O_2 production, a comprehensive understanding of the photocatalytic mechanism for H_2O_2 production is necessary. Both experimental and theoretical investigations should be simultaneously carried out. In situ measurements by Kelvin probe microscopy (Zhu J. et al., 2015) and X-ray absorption fine structure analysis (Yang H. et al., 2018) could be used to study the dynamic behavior of photogenerated carriers on the surface and the changes of oxidized states in a photocatalyst (Hou H. et al., 2020). In situ Raman spectroscopy may reveal the process from the adsorption of O_2 to dissociation of H_2O_2, thus leading to a more precise understanding of the mechanism. In the case of fundamental calculations and simulations for investigation of the mechanism, ground state properties such as density of states, adsorption energy, and the structural and electronic properties have been widely used for explanation of physicochemical properties for the design of an ideal photocatalyst for H_2O_2 production (Dong J.-C. et al., 2020). However, investigation of the excitation properties of PCN materials has not been sufficient to obtain a fundamental understanding of the excitation behavior of a photocatalyst. We suggest that excitation properties of the functionalized PCN, such as transition densities based on time-dependent DFT calculations (Laurent A.D. et al., 2013; Teng Z. et al., 2021b; Che H. et al., 2021), should be investigated in future studies in order to establish a satisfactory blueprint for designing a PCN catalyst for H_2O_2 production. Last but not least, since H_2O_2 production is a green oxidant for many chemical reactions, the development of highly value-added chemicals based on the photocatalytic systems is needed. Using the in-situ generated H_2O_2 for synthesis of chemicals could also be achieved on the basis of previous work using D_2O to produce deuterated chemicals (Zhang B. et al., 2021). We believe that better design strategies and guidelines for not only PCN-based materials but also other efficient photocatalysts can be established for H_2O_2 formation if the above-mentioned properties can be achieved.

Acknowledgements

The authors acknowledge the financial support of Mitsubishi Chemical Corporation, JSPS Grant-in-Aid for Scientific Research (B, No. 20H02847), and Grant-in-Aid for JSPS Fellows (DC2, 20J13064).

References

Banerjee T., Podjaski F., Kröger J., Biswal B.P., Lotsch B.V., Polymer photocatalysts for solar-to-chemical energy conversion, Nature Reviews Materials, 6 (2021) 168–190. DOI: 10.1038/s41578-020-00254-z

Bo Y., Gao C., Xiong Y., Recent advances in engineering active sites for photocatalytic CO_2 reduction, Nanoscale, 12 (2020) 12196–12209. DOI: 10.1039/D0NR02596H

Campos-Martin J.M., Blanco-Brieva G., Fierro J.L.G., Hydrogen peroxide synthesis: an outlook beyond the anthraquinone process, Angewandte Chemie International Edition, 45 (2006) 6962–6984. DOI: 10.1002/anie.200503779

Chang X., Yang J., Han D., Zhang B., Xiang X., He J., Enhancing light-driven production of hydrogen peroxide by anchoring Au onto C_3N_4 catalysts, Catalysts, 8 (2018) 147. DOI: 10.3390/catal8040147

Che H., Gao X., Chen J., Hou J., Ao Y., Wang P., Iodide-induced fragmentation of polymerized hydrophilic carbon nitride for high-performance quasi-homogeneous photocatalytic H_2O_2 production, Angewandte Chemie International Edition, 60 (2021) 25546–25550. DOI: 10.1002/anie.202111769

Choi C.H., Kwon H.C., Yook S., Shin H., Kim H., Choi M., Hydrogen peroxide synthesis via enhanced two-electron oxygen reduction pathway on carbon-coated Pt surface, The Journal of Physical Chemistry C, 118 (2014) 30063–30070. DOI: 10.1021/jp5113894

Chu C., Huang D., Zhu Q., Stavitski E., Spies J.A., Pan Z., Mao J., Xin H.L., Schmuttenmaer C.A., Hu S., Kim J.-H., Electronic tuning of metal nanoparticles for highly efficient photocatalytic hydrogen peroxide production, ACS Catalysis, 9 (2019) 626–631. DOI: 10.1021/acscatal.8b03738

Chu C., Zhu Q., Pan Z., Gupta S., Huang D., Du Y., Weon S., Wu Y., Muhich C., Stavitski E., Domen K., Kim J.-H., Spatially separating redox centers on 2D carbon nitride with cobalt single atom for photocatalytic H_2O_2 production, Proceedings of the National Academy of Sciences of the United States of America, 117 (2020) 6376. DOI: 10.1073/pnas.1913403117

Chung D.D.L., Carbon Materials: Science and Applications, World Scientific Publishing Company, 2019, ISBN: 9789811200939.

Dong J.-C., Su M., Briega-Martos V., Li L., Le J.-B., Radjenovic P., Zhou X.-S., Feliu J.M., Tian Z.-Q., Li J.-F., Direct in situ Raman spectroscopic evidence of oxygen reduction reaction intermediates at high-index Pt(hkl) surfaces, Journal of the American Chemical Society, 142 (2020) 715–719. DOI: 10.1021/jacs.9b12803

Fan W., Zhang B., Wang X., Ma W., Li D., Wang Z., Dupuis M., Shi J., Liao S., Li C., Efficient hydrogen peroxide synthesis by metal-free polyterthiophene via photoelectrocatalytic

dioxygen reduction, Energy & Environmental Science, 13 (2020) 238–245. DOI: 10.1039/C9EE02247C

Freakley S.J., He Q., Harrhy J.H., Lu L., Crole D.A., Morgan D.J., Ntainjua E.N., Edwards J.K., Carley A.F., Borisevich A.Y., Kiely C.J., Hutchings G.J., Palladium-tin catalysts for the direct synthesis of H_2O_2 with high selectivity, Science, 351 (2016) 965. DOI: 10.1126/science.aad5705

Fuku K., Sayama K., Efficient oxidative hydrogen peroxide production and accumulation in photoelectrochemical water splitting using a tungsten trioxide/bismuth vanadate photoanode, Chemical Communications, 52 (2016) 5406–5409. DOI: 10.1039/C6CC01605G

Gao J., Liu B., Progress of electrochemical hydrogen peroxide synthesis over single atom catalysts, ACS Materials Letters, 2 (2020) 1008–1024. DOI: 10.1021/acsmaterialslett.0c00189

Gao J., Yang H.b., Huang X., Hung S.-F., Cai W., Jia C., Miao S., Chen H.M., Yang X., Huang Y., Zhang T., Liu B., Enabling direct H_2O_2 production in acidic media through rational design of transition metal single atom catalyst, Chem, 6 (2020) 658–674. DOI: 10.1016/j.chempr.2019.12.008

Goclon J., Winkler K., Computational insight into the mechanism of O_2 to H_2O_2 reduction on amino-groups-containing g-C_3N_4, Applied Surface Science, 462 (2018) 134–141. DOI: 10.1016/j.apsusc.2018.08.070

Han X.-B., Li Y.-G., Zhang Z.-M., Tan H.-Q., Lu Y., Wang E.-B., Polyoxometalate-based nickel clusters as visible light-driven water oxidation catalysts, Journal of the American Chemical Society, 137 (2015) 5486–5493. DOI: 10.1021/jacs.5b01329

Hirakawa H., Shiota S., Shiraishi Y., Sakamoto H., Ichikawa S., Hirai T., Au nanoparticles supported on $BiVO_4$: effective inorganic photocatalysts for H_2O_2 production from water and O_2 under visible light, ACS Catalysis, 6 (2016) 4976–4982. DOI: 10.1021/acscatal.6b01187

Hisatomi T., Domen K., Reaction systems for solar hydrogen production via water splitting with particulate semiconductor photocatalysts, Nature Catalysis, 2 (2019) 387–399. DOI: 10.1038/s41929-019-0242-6

Hou H., Zeng X., Zhang X., Production of hydrogen peroxide by photocatalytic processes, Angewandte Chemie International Edition, 59 (2020) 17356–17376. DOI: 10.1002/anie.201911609

Hu S., Qu X., Li P., Wang F., Li Q., Song L., Zhao Y., Kang X., Photocatalytic oxygen reduction to hydrogen peroxide over copper doped graphitic carbon nitride hollow microsphere: the effect of Cu(I)-N active sites, Chemical Engineering Journal, 334 (2018) 410–418. DOI: 10.1016/j.cej.2017.10.016

Iglesias D., Giuliani A., Melchionna M., Marchesan S., Criado A., Nasi L., Bevilacqua M., Tavagnacco C., Vizza F., Prato M., Fornasiero P., N-doped graphitized carbon nanohorns as a forefront electrocatalyst in highly selective O_2 Reduction to H_2O_2, Chem, 4 (2018) 106–123. DOI: 10.1016/j.chempr.2017.10.013

Inoue Y., Photocatalytic water splitting by RuO_2-loaded metal oxides and nitrides with d^0- and d^{10} -related electronic configurations, Energy & Environmental Science, 2 (2009) 364–386. DOI: 10.1039/B816677N

Jiang X., Wang P., Zhao J., 2D covalent triazine framework: a new class of organic photocatalyst for water splitting, Journal of Materials Chemistry A, 3 (2015) 7750–7758. DOI: 10.1039/C4TA03438D

Jones C.W., Applications of hydrogen peroxide and derivatives, Royal Society of Chemistry, 1999, ISSN: 978-0-85404-536-5

Jung E., Shin H., Lee B.-H., Efremov V., Lee S., Lee H., Kim J., Antink W., Park S., Lee K.-S., Cho S.-P., Yoo J.S., Sung Y.-E., Hyeon T., Atomic-level tuning of Co–N–C catalyst for high-performance electrochemical H_2O_2 production, Nature Materials, 19 (2020) 1–7. DOI: 10.1038/s41563-019-0571-5

Kessler F.K., Zheng Y., Schwarz D., Merschjann C., Schnick W., Wang X., Bojdys M.J., Functional carbon nitride materials—design strategies for electrochemical devices, Nature Reviews Materials, 2 (2017) 17030. DOI: 10.1038/natrevmats.2017.30

Kim D., Sakimoto K.K., Hong D., Yang P., Artificial photosynthesis for sustainable fuel and chemical production, Angewandte Chemie International Edition, 54 (2015) 3259–3266. DOI: 10.1002/anie.201409116

Kim H.-i., Choi Y., Hu S., Choi W., Kim J.-H., Photocatalytic hydrogen peroxide production by anthraquinone-augmented polymeric carbon nitride, Applied Catalysis B: Environmental, 229 (2018) 121–129. DOI: 10.1016/j.apcatb.2018.01.060

Kim H.W., Ross M.B., Kornienko N., Zhang L., Guo J., Yang P., McCloskey B.D., Efficient hydrogen peroxide generation using reduced graphene oxide-based oxygen reduction electrocatalysts, Nature Catalysis, 1 (2018) 282–290. DOI: 10.1038/s41929-018-0044-2

Kim S., Moon G.-h., Kim H., Mun Y., Zhang P., Lee J., Choi W., Selective charge transfer to dioxygen on KPF_6-modified carbon nitride for photocatalytic synthesis of H_2O_2 under visible light, Journal of Catalysis, 357 (2018) 51–58. DOI: 10.1016/j.jcat.2017.10.002

Koe W.S., Lee J.W., Chong W.C., Pang Y.L., Sim L.C., An overview of photocatalytic degradation: photocatalysts, mechanisms, and development of photocatalytic membrane, Environmental Science and Pollution Research, 27 (2020) 2522–2565. DOI: 10.1007/s11356-019-07193-5

Kofuji Y., Isobe Y., Shiraishi Y., Sakamoto H., Ichikawa S., Tanaka S., Hirai T., Hydrogen peroxide production on a carbon nitride–boron nitride-reduced graphene oxide hybrid photocatalyst under visible light, ChemCatChem, 10 (2018) 2070–2077. DOI: 10.1002/cctc.201701683

Kofuji Y., Isobe Y., Shiraishi Y., Sakamoto H., Tanaka S., Ichikawa S., Hirai T., Carbon nitride–aromatic diimide–graphene nanohybrids: Metal-free photocatalysts for solar-to-hydrogen peroxide energy conversion with 0.2 % efficiency, Journal of the American Chemical Society, 138 (2016a) 10019–10025. DOI: 10.1021/jacs.6b05806

Kofuji Y., Ohkita S., Shiraishi Y., Sakamoto H., Ichikawa S., Tanaka S., Hirai T., Mellitic triimide-doped carbon nitride as sunlight-driven photocatalysts for hydrogen peroxide production, ACS Sustainable Chemistry & Engineering, 5 (2017) 6478–6485. DOI: 10.1021/acssuschemeng.7b00575

Kofuji Y., Ohkita S., Shiraishi Y., Sakamoto H., Tanaka S., Ichikawa S., Hirai T., Graphitic carbon nitride doped with biphenyl diimide: efficient photocatalyst for hydrogen peroxide production from water and molecular oxygen by sunlight, ACS Catalysis, 6 (2016b) 7021–7029. DOI: 10.1021/acscatal.6b02367

Kulkarni A., Siahrostami S., Patel A., Nørskov J.K., Understanding catalytic activity trends in the oxygen reduction reaction, Chemical Reviews, 118 (2018) 2302–2312. DOI: 10.1021/acs.chemrev.7b00488

Kuo W.G., Decolorizing dye wastewater with Fenton's reagent., Water Research, 26 (1992) 881–886. DOI: 10.1016/0043-1354(92)90192-7

Laurent A.D., Jacquemin D., TD-DFT benchmarks: a review, International Journal of Quantum Chemistry, 113 (2013) 2019–2039. DOI: 10.1002/qua.24438

Li S., Dong G., Hailili R., Yang L., Li Y., Wang F., Zeng Y., Wang C., Effective photocatalytic H_2O_2 production under visible light irradiation at g-C_3N_4 modulated by carbon vacancies,

Applied Catalysis B: Environmental, 190 (2016) 26–35. DOI: 10.1016/j.apcatb.2016.03.004

Li X., Chen C., Zhao J., Mechanism of photodecomposition of H_2O_2 on TiO_2 surfaces under visible light irradiation, Langmuir, 17 (2001) 4118–4122. DOI: 10.1021/la010035s

Li X., Sun X., Zhang L., Sun S., Wang W., Efficient photocatalytic fixation of N_2 by KOH-treated g-C_3N_4, Journal of Materials Chemistry A, 6 (2018a) 3005–3011. DOI: 10.1039/C7TA09762J

Li X., Zhang J., Zhou F., Zhang H., Bai J., Wang Y., Wang H., Preparation of N-vacancy-doped g-C_3N_4 with outstanding photocatalytic H_2O_2 production ability by dielectric barrier discharge plasma treatment, Chinese Journal of Catalysis, 39 (2018b) 1090–1098. DOI: 10.1016/S1872-2067(18)63046-3

Liao G., Gong Y., Zhang L., Gao H., Yang G.-J., Fang B., Semiconductor polymeric graphitic carbon nitride photocatalysts: the "holy grail" for the photocatalytic hydrogen evolution reaction under visible light, Energy & Environmental Science, 12 (2019) 2080–2147. DOI: 10.1039/C9EE00717B

Liu L., Gao M.-Y., Yang H., Wang X., Li X., Cooper A.I., Linear conjugated polymers for solar-driven hydrogen peroxide production: the importance of catalyst stability, Journal of the American Chemical Society, 143 (2021) 19287–19293. DOI: 10.1021/jacs.1c09979

Liu R., Chen Z., Yao Y., Li Y., Cheema A.W., Wang D., Zhu S., Recent advancements in g-C_3N_4-based photocatalysts for photocatalytic CO_2 reduction: a mini review, RSC Advances, 10 (2020) 29408–29418. DOI: 10.1039/D0RA05779G

Liu X., Ma R., Zhuang L., Hu B., Chen J., Liu X., Wang X., Recent developments of doped g-C_3N_4 photocatalysts for the degradation of organic pollutants, Critical Reviews in Environmental Science and Technology, (2020) 1–40. DOI: 10.1080/10643389.2020.1734433

Lu Z., Chen G., Siahrostami S., Chen Z., Liu K., Xie J., Liao L., Wu T., Lin D., Liu Y., Jaramillo T.F., Nørskov J.K., Cui Y., High-efficiency oxygen reduction to hydrogen peroxide catalysed by oxidized carbon materials, Nature Catalysis, 1 (2018) 156–162. DOI: 10.1038/s41929-017-0017-x

McDonnell G., The use of hydrogen peroxide for disinfection and sterilization applications, PATAI'S Chemistry of Functional Groups, (2014) 1–34. DOI: 10.1002/9780470682531.pat0885

Meng A., Teng Z., Zhang Q., Su C., Intrinsic defects in polymeric carbon nitride for photocatalysis applications, Chemistry–An Asian Journal, 15 (2020) 3405–3415. DOI: 10.1002/asia.202000850

Mohamed N.A., Safaei J., Ismail A.F., Jailani M.F.A.M., Khalid M.N., Noh M.F.M., Aadenan A., Nasir S.N.S.N., Sagu J.S., Teridi M.S.M., The influences of post-annealing temperatures on fabrication graphitic carbon nitride, (g-C_3N_4) thin film, Applied Surface Science, (2019) 92–100. DOI: 10.1016/j.apsusc.2019.05.312.

Moon G.-h., Fujitsuka M., Kim S., Majima T., Wang X., Choi W., Eco-friendly photochemical production of H_2O_2 through O_2 reduction over carbon nitride frameworks incorporated with multiple heteroelements, ACS Catalysis, 7 (2017) 2886–2895. DOI: 10.1021/acscatal.6b03334

Mousavi Shaegh S.A., Nguyen N.-T., Mousavi Ehteshami S.M., Chan S.H., A membraneless hydrogen peroxide fuel cell using Prussian Blue as cathode material, Energy & Environmental Science, 5 (2012) 8225–8228. DOI: 10.1039/C2EE21806B

Nosaka Y., Nosaka A., Introduction to Photocatalysis: From Basic Science to Applications, 1st edition, Royal Society of Chemistry, 2016, ISBN: 1782623205.

Ong W.-J., Tan L.-L., Ng Y.H., Yong S.-T., Chai S.-P., Graphitic carbon nitride (g-C_3N_4)-based photocatalysts for artificial photosynthesis and environmental remediation: are we a step closer to achieving sustainability?, Chemical Reviews, 116 (2016) 7159–7329. DOI: 10.1021/acs.chemrev.6b00075

Ou H., Yang P., Lin L., Anpo M., Wang X., Carbon nitride aerogels for the photoredox conversion of water, Angewandte Chemie International Edition, 56 (2017) 10905–10910. DOI: 10.1002/anie.201705926

Pei Z., Ding L., Hu J, Weng S., Zheng Z., Huang M., Liu P., Defect and its dominance in ZnO films: a new insight into the role of defect over photocatalytic activity, Applied Catalysis B: Environmental, 142–143 (2013) 736–743. DOI: 10.1016/j.apcatb.2013.05.055

Peng Y., Wang L., Liu Y., Chen H., Lei J., Zhang J., Visible-light-driven photocatalytic H_2O_2 production on g-C_3N_4 loaded with CoP as a noble metal free cocatalyst, European Journal of Inorganic Chemistry, 2017 (2017) 4797–4802. DOI: 10.1002/ejic.201700930

Pesterfield L., The 100 most important chemical compounds: a reference guide (by Richard L. Myers), Journal of Chemical Education, 86 (2009) 1182. DOI: 10.1021/ed086p1182

Qiang Z., Chang J.-H., Huang C.P., Electrochemical generation of hydrogen peroxide from dissolved oxygen in acidic solutions, Water Research, 36 (2002) 85–94. DOI: 10.1016/S0043-1354(01)00235-4

Qiu C., Xu Y., Fan X., Xu D., Tandiana R., Ling X., Jiang Y., Liu C., Yu L., Chen W., Su C., Highly crystalline k-intercalated polymeric carbon nitride for visible-light photocatalytic alkenes and alkynes deuterations, Advanced Science, 6 (2019) 1801403. DOI: 10.1002/advs.201801403

Qu X., Hu S., Li P., Li Z., Wang H., Ma H., Li W., The effect of embedding N vacancies into g-C_3N_4 on the photocatalytic H_2O_2 production ability via H_2 plasma treatment, Diamond and Related Materials, 86 (2018) 159–166. DOI: 10.1016/j.diamond.2018.04.027

Schneider J., Bahnemann D.W., Undesired role of sacrificial reagents in photocatalysis, The Journal of Physical Chemistry Letters, 4 (2013) 3479–3483. DOI: 10.1021/jz4018199

Shen R., Chen W., Peng Q., Lu S., Zheng L., Cao X., Wang Y., Zhu W., Zhang J., Zhuang Z., Chen C., Wang D., Li Y., High-concentration single atomic Pt sites on hollow CuSx for selective O_2 reduction to H_2O_2 in acid solution, Chem, 5 (2019) 2099–2110. DOI: 10.1016/j.chempr.2019.04.024

Shi L., Yang L., Zhou W., Liu Y., Yin L., Hai X., Song H., Ye J., Photoassisted construction of holey defective g-C_3N_4 photocatalysts for efficient visible-light-driven H_2O_2 production, Small, 14 (2018) 1703142. DOI: 10.1002/smll.201703142

Shi X., Siahrostami S., Li G.-L., Zhang Y., Chakthranont P., Studt F., Jaramillo T.F., Zheng X., Nørskov J.K., Understanding activity trends in electrochemical water oxidation to form hydrogen peroxide, Nature Communications, 8 (2017) 701. DOI: 10.1038/s41467-017-00585-6

Shiraishi Y., Kanazawa S., Kofuji Y., Sakamoto H., Ichikawa S., Tanaka S., Hirai T., Sunlight-driven hydrogen peroxide production from water and molecular oxygen by metal-free photocatalysts, Angewandte Chemie International Edition, 53 (2014a) 13454–13459. DOI: 10.1002/anie.201407938

Shiraishi Y., Kanazawa S., Sugano Y., Tsukamoto D., Sakamoto H., Ichikawa S., Hirai T., Highly selective production of hydrogen peroxide on graphitic carbon nitride (g-C_3N_4) photocatalyst activated by visible light, ACS Catalysis, 4 (2014b) 774–780. DOI: 10.1021/cs401208c

Shiraishi Y., Kofuji Y., Sakamoto H., Tanaka S., Ichikawa S., Hirai T., Effects of surface defects on photocatalytic H_2O_2

production by mesoporous graphitic carbon nitride under visible light irradiation, ACS Catalysis, 5 (2015) 3058–3066. DOI: 10.1021/acscatal.5b00408

Shiraishi Y., Takii T., Hagi T., Mori S., Kofuji Y., Kitagawa Y., Tanaka S., Ichikawa S., Hirai T., Resorcinol–formaldehyde resins as metal-free semiconductor photocatalysts for solar-to-hydrogen peroxide energy conversion, Nature Materials, 18 (2019) 985–993. DOI: 10.1038/s41563-019-0398-0

Siahrostami S., Verdaguer-Casadevall A., Karamad M., Deiana D., Malacrida P., Wickman B., Escudero-Escribano M., Paoli E.A., Frydendal R., Hansen T.W., Chorkendorff I., Stephens I.E.L., Rossmeisl J., Enabling direct H_2O_2 production through rational electrocatalyst design, Nature Materials, 12 (2013) 1137–1143. DOI: 10.1038/nmat3795

Sun H., Ma Y., Zhang Q., Su C., Engineering the local coordination environment of single-atom catalysts and their applications in photocatalytic water splitting: a review, Transactions of Tianjin University, 27 (2021) 313–330. DOI: 10.1007/s12209-021-00295-7

Sun S., Li J., Cui J., Gou X., Yang Q., Jiang Y., Liang S., Yang Z., Simultaneously engineering K-doping and exfoliation into graphitic carbon nitride (g-C_3N_4) for enhanced photocatalytic hydrogen production, International Journal of Hydrogen Energy, 44 (2019) 778–787. DOI: 10.1016/j.ijhydene.2018.11.019

Tasis D., Tagmatarchis N., Bianco A., Prato M., Chemistry of carbon nanotubes, Chemical Reviews, 106 (2006) 1105–1136. DOI: 10.1021/cr050569o

Teixeira I.F., Barbosa E.C.M., Tsang S.C.E., Camargo P.H.C., Carbon nitrides and metal nanoparticles: from controlled synthesis to design principles for improved photocatalysis, Chemical Society Reviews, 47 (2018) 7783–7817. DOI: 10.1039/C8CS00479J

Teng Z., Cai W., Liu S., Wang C., Zhang Q., Chenliang S., Ohno T., Bandgap engineering of polymetric carbon nitride copolymerized by 2,5,8-triamino-tri-s-triazine (melem) and barbituric acid for efficient nonsacrificial photocatalytic H_2O_2 production, Applied Catalysis B: Environmental, 271 (2020) 118917. DOI: 10.1016/j.apcatb.2020.118917

Teng Z., Cai W., Sim W., Zhang Q., Wang C., Su C., Ohno T., Photoexcited single metal atom catalysts for heterogeneous photocatalytic H_2O_2 production: Pragmatic guidelines for predicting charge separation, Applied Catalysis B: Environmental, 282 (2021a) 119589. DOI: 10.1016/j.apcatb.2020.119589

Teng Z., Lv H., Wang C., Xue H., Pang H., Wang G., Bandgap engineering of ultrathin graphene-like carbon nitride nanosheets with controllable oxygenous functionalization, Carbon, 113 (2017) 63–75. DOI: 10.1016/j.carbon.2016.11.030

Teng Z., Yang N., Lv H., Wang S., Hu M., Wang C., Wang D., Wang G., Edge-functionalized g-C_3N_4 nanosheets as a highly efficient metal-free photocatalyst for safe drinking water, Chem, 5 (2019) 664–680. DOI: 10.1016/j.chempr.2018.12.009

Teng Z., Zhang Q., Yang H., Kato K., Yang W., Lu Y.-R., Liu S., Wang C., Yamakata A., Su C., Liu B., Ohno T., Atomically dispersed antimony on carbon nitride for the artificial photosynthesis of hydrogen peroxide, Nature Catalysis, 4 (2021b) 374–384. DOI: 10.1038/s41929-021-00605-1

Thakur S., Kshetri T., Kim N.H., Lee J.H., Sunlight-driven sustainable production of hydrogen peroxide using a CdS–graphene hybrid photocatalyst, Journal of Catalysis, 345 (2017) 78–86. DOI: 10.1016/j.jcat.2016.10.028

Torres-Pinto A., Sampaio M.J., Silva C.G., Faria J.L., Silva M.T.A., Recent strategies for hydrogen peroxide production by metal-free carbon nitride photocatalysts, Catalysts, 9 (2019) 990. DOI: 10.3390/catal9120990

Tsukamoto D., Shiro A., Shiraishi Y., Sugano Y., Ichikawa S., Tanaka S., Hirai T., Photocatalytic H_2O_2 production from ethanol/O_2 system using TiO_2 loaded with Au–Ag bimetallic alloy nanoparticles, ACS Catalysis, 2 (2012) 599–603. DOI: 10.1021/cs2006873

Verdaguer-Casadevall A., Deiana D., Karamad M., Siahrostami S., Malacrida P., Hansen T.W., Rossmeisl J., Chorkendorff I., Stephens I.E.L., Trends in the electrochemical synthesis of H_2O_2: enhancing activity and selectivity by electrocatalytic site engineering, Nano Letters, 14 (2014) 1603–1608. DOI: 10.1021/nl500037x

Wang A., Li J., Zhang T., Heterogeneous single-atom catalysis, Nature Reviews Chemistry, 2 (2018) 65–81. DOI: 10.1038/s41570-018-0010-1

Wang M., Shen S., Li L., Tang Z., Yang J., Effects of sacrificial reagents on photocatalytic hydrogen evolution over different photocatalysts, Journal of Materials Science, 52 (2017) 5155–5164. DOI: 10.1007/s10853-017-0752-z

Wang Q., Domen K., Particulate photocatalysts for light-driven water splitting: mechanisms, challenges, and design strategies, Chemical Reviews, 120 (2020) 919–985. DOI: 10.1021/acs.chemrev.9b00201

Wang S., Teng Z., Xu Y., Yuan M., Zhong Y., Liu S., Wang C., Wang G., Ohno T., Defect as the essential factor in engineering carbon-nitride-based visible-light-driven Z-scheme photocatalyst, Applied Catalysis B: Environmental, 260 (2020a) 118145. DOI: 10.1016/j.apcatb.2019.118145

Wang S., Zhan J., Chen K., Ali A., Zeng L., Zhao H., Hu W., Zhu L., Xu X., Potassium-doped g-C_3N_4 achieving efficient visible-light-driven CO_2 Reduction, ACS Sustainable Chemistry & Engineering, 8 (2020b) 8214–8222. DOI: 10.1021/acssuschemeng.0c01151

Wang X., Maeda K., Thomas A., Takanabe K., Xin G., Carlsson J.M., Domen K., Antonietti M., A metal-free polymeric photocatalyst for hydrogen production from water under visible light, Nature Materials, 8 (2009) 76–80. DOI: 10.1038/nmat2317

Wang Y., Vogel A., Sachs M., Sprick R.S., Wilbraham L., Moniz S.J.A., Godin R., Zwijnenburg M.A., Durrant J.R., Cooper A.I., Tang J., Current understanding and challenges of solar-driven hydrogen generation using polymeric photocatalysts, Nature Energy, 4 (2019) 746–760. DOI: 10.1038/s41560-019-0456-5

Wei Y., Zhang J., Zheng Q., Miao J., Alvarez P.J., Long M., Quantification of photocatalytically-generated hydrogen peroxide in the presence of organic electron donors: interference and reliability considerations, Chemosphere, 279 (2021) 130556. DOI: 10.1016/j.chemosphere.2021.130556

Wei Z., Liu M., Zhang Z., Yao W., Tan H., Zhu Y., Efficient visible-light-driven selective oxygen reduction to hydrogen peroxide by oxygen-enriched graphitic carbon nitride polymers, Energy & Environmental Science, 11 (2018) 2581–2589. DOI: 10.1039/C8EE01316K

Xia C., Xia Y., Zhu P., Fan L., Wang H., Direct electrosynthesis of pure aqueous H_2O_2 solutions up to 20 % by weight using a solid electrolyte, Science, 366 (2019) 226. DOI: 10.1126/science.aay1844

Xiong J., Di J., Xia J., Zhu W., Li H., Surface defect engineering in 2D nanomaterials for photocatalysis, Advanced Functional Materials, 28 (2018) 1801983. DOI: 10.1002/adfm.201801983

Xu Q., Zhang L., Yu J., Wageh S., Al-Ghamdi A.A., Jaroniec M., Direct Z-scheme photocatalysts: principles, synthesis, and

applications, Materials Today, 21 (2018) 1042–1063. DOI: 10.1016/j.mattod.2018.04.008

Yamada Y., Yoneda M., Fukuzumi S., A robust one-compartment fuel cell with a polynuclear cyanide complex as a cathode for utilizing H_2O_2 as a sustainable fuel at ambient conditions, Chemistry – A European Journal, 19 (2013) 11733–11741. DOI: 10.1002/chem.201300783

Yang H.B., Hung S.-F., Liu S., Yuan K., Miao S., Zhang L., Huang X., Wang H.-Y., Cai W., Chen R., Gao J., Yang X., Chen W., Huang Y., Chen H.M., et al., Atomically dispersed Ni(i) as the active site for electrochemical CO_2 reduction, Nature Energy, 3 (2018) 140–147. DOI: 10.1038/s41560-017-0078-8

Yang L., Dong G., Jacobs D.L., Wang Y., Zang L., Wang C., Two-channel photocatalytic production of H_2O_2 over g-C_3N_4 nanosheets modified with perylene imides, Journal of Catalysis, 352 (2017) 274–281. DOI: 10.1016/j.jcat.2017.05.010

Yang S., Verdaguer-Casadevall A., Arnarson L., Silvioli L., Čolić V., Frydendal R., Rossmeisl J., Chorkendorff I., Stephens I.E.L., Toward the decentralized electrochemical production of H_2O_2: a focus on the catalysis, ACS Catalysis, 8 (2018) 4064–4081. DOI: 10.1021/acscatal.8b00217

Yi Y., Wang L., Li G., Guo H., A review on research progress in the direct synthesis of hydrogen peroxide from hydrogen and oxygen: noble-metal catalytic method, fuel-cell method and plasma method, Catalysis Science and Technology, 6 (2016) 1593–1610. DOI: 10.1039/C5CY01567G

Zeng X., Liu Y., Kang Y., Li Q., Xia Y., Zhu Y., Hou H., Uddin M.H., Gengenbach T.R., Xia D., Sun C., Mccarthy D.T., Deletic A., Yu J., Zhang X., Simultaneously tuning charge separation and oxygen reduction pathway on graphitic carbon nitride by polyethylenimine for boosted photocatalytic hydrogen peroxide production, ACS Catalsis, 10 (2020) 3697–3706. DOI: 10.1021/acscatal.9b05247

Zeng X., Wang Z., Meng N., McCarthy D.T., Deletic A., Pan J.-h., Zhang X., Highly dispersed TiO_2 nanocrystals and carbon dots on reduced graphene oxide: ternary nanocomposites for accelerated photocatalytic water disinfection, Applied Catalysis B: Environmental, 202 (2017) 33–41. DOI: 10.1016/j.apcatb.2016.09.014

Zhan W., Ji L., Ge Z.-m., Wang X., Li R.-t., A continuous-flow synthesis of primary amides from hydrolysis of nitriles using hydrogen peroxide as oxidant, Tetrahedron, 74 (2018) 1527–1532. DOI: 10.1016/j.tet.2018.02.017

Zhang B., Qiu C., Wang S., Gao H., Yu K., Zhang Z., Ling X., Ou W., Su C., Electrocatalytic water-splitting for the controllable and sustainable synthesis of deuterated chemicals, Science Bulletin, 66 (2021) 562–569. DOI: 10.1016/j.scib.2020.09.016

Zhang C., Bai J., Ma L., Lv Y., Wang F., Zhang X., Yuan X., Hu S., Synthesis of halogen doped graphite carbon nitride nanorods with outstanding photocatalytic H_2O_2 production ability via saturated NH_4X (X = Cl, Br) solution-hydrothermal post-treatment, Diamond and Related Materials, 87 (2018) 215–222. DOI: 10.1016/j.diamond.2018.06.013

Zhang G., Yang X., He C., Zhang P., Mi H., Constructing a tunable defect structure in TiO_2 for photocatalytic nitrogen fixation, Journal of Materials Chemistry A, 8 (2020) 334–341. DOI: 10.1039/C9TA10471B

Zhang M.-h., Dong H., Zhao L., Wang D.-x., Meng D., A review on Fenton process for organic wastewater treatment based on optimization perspective, Science of the Total Environment, 670 (2019) 110–121. DOI: 10.1016/j.scitotenv.2019.03.180

Zhang P., Sun D., Cho A., Weon S., Lee S., Lee J., Han J.W., Kim D.-P., Choi W., Modified carbon nitride nanozyme as bifunctional glucose oxidase-peroxidase for metal-free bioinspired cascade photocatalysis, Nature Communications, 10 (2019) 940. DOI: 10.1038/s41467-019-08731-y

Zhang P., Tong Y., Liu Y., Vequizo J.J.M., Sun H., Yang C., Yamakata A., Fan F., Lin W., Wang X., Heteroatom dopants promote two-electron O_2 reduction for photocatalytic production of H_2O_2 on polymeric carbon nitride, Angewandte Chemie, 132 (2020) 16343–16351. DOI: 10.1002/ange.202006747

Zhang Z., Xu Y., Zhang Q., Fang S., Sun H., Ou W., Su C. Semi-heterogeneous photo-Cu-dual-catalytic cross-coupling reactions using polymeric carbon nitrides. Science Bulletin, 67 (2022) 71–78. DOI: 10.1016/j.scib.2021.08.001

Zhang Z., Yates J.T., Band bending in semiconductors: Chemical and physical consequences at surfaces and interfaces, Chemical Reviews, 112 (2012) 5520–5551. DOI: 10.1021/cr3000626

Zhao S., Guo T., Li X., Xu T., Yang B., Zhao X., Carbon nanotubes covalent combined with graphitic carbon nitride for photocatalytic hydrogen peroxide production under visible light, Applied Catalysis B: Environmental, 224 (2018a) 725–732. DOI: 10.1016/j.apcatb.2017.11.005

Zhao S., Zhao X., Insights into the role of singlet oxygen in the photocatalytic hydrogen peroxide production over polyoxometalates-derived metal oxides incorporated into graphitic carbon nitride framework, Applied Catalysis B: Environmental, 250 (2019) 408–418. DOI: 10.1016/j.apcatb.2019.02.031

Zhao S., Zhao X., Ouyang S., Zhu Y., Polyoxometalates covalently combined with graphitic carbon nitride for photocatalytic hydrogen peroxide production, Catalysis Science and Technology, 8 (2018b) 1686–1695. DOI: 10.1039/C8CY00043C

Zhao S., Zhao X., Zhang H., Li J., Zhu Y., Covalent combination of polyoxometalate and graphitic carbon nitride for light-driven hydrogen peroxide production, Nano Energy, 35 (2017) 405–414. DOI: 10.1016/j.nanoen.2017.04.017

Zhu J., Fan F., Chen R., An H., Feng Z., Li C., Direct imaging of highly anisotropic photogenerated charge separations on different facets of a single $BiVO_4$ photocatalyst, Angewandte Chemie International Edition, 54 (2015) 9111–9114. DOI: 10.1002/anie.201504135

Zhu Z., Pan H., Murugananthan M., Gong J., Zhang Y., Visible light-driven photocatalytically active g-C_3N_4 material for enhanced generation of H_2O_2, Applied Catalysis B: Environmental, 232 (2018) 19–25. DOI: 10.1016/j.apcatb.2018.03.035

Zuo G., Liu S., Wang L., Song H., Zong P., Hou W., Li B., Guo Z., Meng X., Du Y., Wang T., Roy V.A.L., Finely dispersed Au nanoparticles on graphitic carbon nitride as highly active photocatalyst for hydrogen peroxide production, Catalysis Communications, 123 (2019) 69–72. DOI: 10.1016/j.catcom.2019.02.011

Authors' Short Biographies

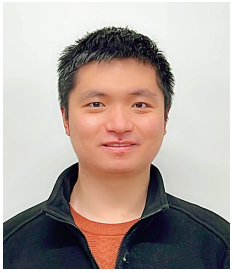

Zhenyuan Teng

Dr. Zhenyuan Teng is currently a JSPS Research Fellow (PD) in the Research Initiative for Supra-Materials (RISM), Interdisciplinary Cluster for Cutting Edge Research, Shinshu University. He obtained his B.S. degree in 2016 and then acquired the Master degree (2018) from Yangzhou University. He obtained his Doctoral degree from Kyushu Institute of Technology in 2021 under the supervision of Prof. Teruhisa Ohno. His research interest focuses on the design and synthesis of single-atom organic-inorganic photocatalytic systems for energetic and environmental applications.

Wenan Cai

Wenan Cai received his B.S. in Beijing Institute of Petrochemical Technology in 2016. Currently, he is a Ph.D. student under the supervision of Prof. Ohno Teruhisa in Kyushu Institute of Technology. His research interest is the development and design of long-wavelength response photocatalysts for H_2O_2 production.

Teruhisa Ohno

Prof. Teruhisa Ohno is currently the dean of faculty of engineering in Kyushu Institute of Technology. He obtained his Doctoral degree in Kyushu University in 1988. He worked as an Associate Professor in Kyushu University from 1992 to 1994 and in Osaka University from 1994–2003. Then he moved to Kyushu Institute of Technology as a Full Professor. From 2016 to 2021, He published 57 SCI papers. Field-Weighted Citation Impact: 2.04, Citation Count: 1,108, h-index: 48, h5-index: 15. A number of papers have published on influential periodical, such as Applied Catalysis B: Environmental, ACS catalysis and Nature Catalysis. From 1983 to now, published about 202 SCI papers, these papers were totally quoted more than 11,763 times and h-index is 49 (Scopus Data). His research interests are: 1. Development of visible light sensitive photocatalysts; 2. Nanoscale surface structure control of TiO_2 photocatalysts; 3. Development of photocatalyst and photoelectrode system for CO_2 reduction; 4. Visible light responsive photocatalyst and photoelectrode for H_2O_2 production.